WT-1648(EX)
EXTRACTED VERSION

OPERATION HARDTACK—PROJECT 8.2

Thermal Radiation from High-Altitude Bursts

R. M. Brubaker, Project Officer
H. P. Gauvin J. P. Cahill
A. T. Stair, Jr. D. J. Baker
Air Force Cambridge Research Laboratories
L. G. Hanscom Field
Bedford, MA

E. A. Jones
Cook Research Laboratories
Morton Grove, IL

J. W. Carpenter
American Science and Engineering, Inc.
Cambridge, MA

DTIC
ELECTE
FEB 27 1986
S D
D

6 October 1961

NOTICE:
This is an extract of WT-1648, Operation HARDTACK, Project 8.2.

Approved for public release;
distribution is unlimited.

Extracted version prepared for
Director
DEFENSE NUCLEAR AGENCY
Washington, DC 20305-1000

1 September 1985

AD-A995 390
DTIC FILE COPY

Destroy this report when it is no longer needed. Do not return to sender.

PLEASE NOTIFY THE DEFENSE NUCLEAR AGENCY, ATTN: STTI, WASHINGTON, DC 20305-1000, IF YOUR ADDRESS IS INCORRECT, IF YOU WISH IT DELETED FROM THE DISTRIBUTION LIST, OR IF THE ADDRESSEE IS NO LONGER EMPLOYED BY YOUR ORGANIZATION.

UNCLASSIFIED
SECURITY CLASSIFICATION OF THIS PAGE

AD-A195390

REPORT DOCUMENTATION PAGE

1a REPORT SECURITY CLASSIFICATION UNCLASSIFIED	1b RESTRICTIVE MARKINGS
2a SECURITY CLASSIFICATION AUTHORITY N/A since Unclassified	3 DISTRIBUTION / AVAILABILITY OF REPORT Approved for public release; distribution is unlimited.
2b DECLASSIFICATION / DOWNGRADING SCHEDULE N/A since Unclassified	
4 PERFORMING ORGANIZATION REPORT NUMBER(S)	5 MONITORING ORGANIZATION REPORT NUMBER(S) WT-1648 (EX)
6a NAME OF PERFORMING ORGANIZATION 1-AF Cambridge Research Labs. 2-Cook Research Labs 3-American Science & Eng, Inc. 6b OFFICE SYMBOL (If applicable)	7a NAME OF MONITORING ORGANIZATION Defense Atomic Support Agency
6c ADDRESS (City, State, and ZIP Code) 1-Bedford, MA 2-Morton Grove, IL 3-Cambridge, MA	7b ADDRESS (City, State, and ZIP Code) Washington, DC
8a NAME OF FUNDING / SPONSORING ORGANIZATION 8b OFFICE SYMBOL (If applicable)	9 PROCUREMENT INSTRUMENT IDENTIFICATION NUMBER
8c ADDRESS (City, State, and ZIP Code)	10 SOURCE OF FUNDING NUMBERS PROGRAM ELEMENT NO / PROJECT NO / TASK NO / WORK UNIT ACCESSION NO

11 TITLE (Include Security Classification)
OPERATION HARDTACK—PROJECT 8.2
Thermal Radiation from High-Altitude Bursts, Extracted Version

12 PERSONAL AUTHOR(S) Brubaker, R.M.; Gauvin, H.P.; Stair, A.T., Jr.; Cahill, J.P.; Baker, D.J.; Jones, E.A.; and Carpenter, J.W.

13a TYPE OF REPORT	13b TIME COVERED FROM ____ TO ____	14 DATE OF REPORT (Year, Month, Day)	15 PAGE COUNT
		611006	69

16 SUPPLEMENTARY NOTATION This report has had sensitive military information removed in order to provide an unclassified version for unlimited distribution. The work was performed by the Defense Nuclear Agency in support of the DoD Nuclear Test Personnel Review Program.

17 COSATI CODES		
FIELD	GROUP	SUB-GROUP
18	3	
20	13	

18 SUBJECT TERMS (Continue on reverse if necessary and identify by block number)
Hardtack
Thermal Radiation
High Altitude Bursts
Radiation Measurements
Atmospheric Transmission

19 ABSTRACT (Continue on reverse if necessary and identify by block number)

The objective of this project was to improve the basic understanding of the physics of high altitude nuclear detonations by measuring the thermal radiation from the high-altitude shots Yucca, Orange, and Teak. Spectral irradiances obtained by distant airborne instrumentation are presented as a function of time in four wavelength bands. The measurements are extrapolated to an assumed point source, and these generalized results are discussed.

Simple scaling laws are not sufficient to predict the thermal radiation from a high-altitude nuclear detonation. In particular, the power radiated in the infrared exceeds by a large factor that expected from a black body of dimensions comparable with the visible fireball. This implies the existence of some mechanism that is producing a greater proportion of infrared radiation than would be obtained using the equilibrium black body theory. Keywords:

20 DISTRIBUTION / AVAILABILITY OF ABSTRACT	21 ABSTRACT SECURITY CLASSIFICATION
☒ UNCLASSIFIED/UNLIMITED ☐ SAME AS RPT ☐ DTIC USERS	UNCLASSIFIED
22a NAME OF RESPONSIBLE INDIVIDUAL MARK D. FLOHR	22b TELEPHONE (Include Area Code) (202) 325-7559
	22c OFFICE SYMBOL DNA/ISCM

DD FORM 1473, 84 MAR 83 APR edition may be used until exhausted
All other editions are obsolete

SECURITY CLASSIFICATION OF THIS PAGE
UNCLASSIFIED

OPERATION HARDTACK — PROJECT 8.2

THERMAL RADIATION FROM HIGH-ALTITUDE BURSTS

R. M. Brubaker, Maj, USAF, Project Officer
H. P. Gauvin, Chief, Radiation Effects Br
A. T. Stair, Jr.
J. P. Cahill
D. J. Baker

Air Force Cambridge Research Laboratories
L. G. Hanscom Field
Bedford, Massachusetts

E. A. Jones

Cook Research Laboratories
Morton Grove, Illinois

J. W. Carpenter

American Science and Engineering, Inc.
Cambridge, Massachusetts

FOREWORD

Classified material has been removed in order to make the information available on an unclassified, open publication basis, to any interested parties. The effort to declassify this report has been accomplished specifically to support the Department of Defense Nuclear Test Personnel Review (NTPR) Program. The objective is to facilitate studies of the low levels of radiation received by some individuals during the atmospheric nuclear test program by making as much information as possible available to all interested parties.

The material which has been deleted is either currently classified as Restricted Data or Formerly Restricted Data under the provisions of the Atomic Energy Act of 1954 (as amended), or is National Security Information, or has been determined to be critical military information which could reveal system or equipment vulnerabilities and is, therefore, not appropriate for open publication.

The Defense Nuclear Agency (DNA) believes that though all classified material has been deleted, the report accurately portrays the contents of the original. DNA also believes that the deleted material is of little or no significance to studies into the amounts, or types, of radiation received by any individuals during the atmospheric nuclear test program.

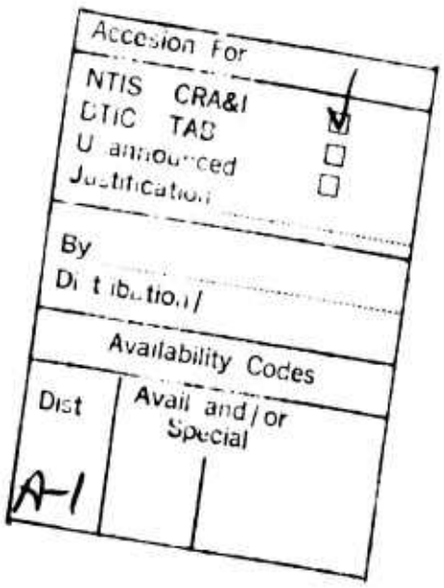

UNANNOUNCED

ABSTRACT

The objective was to improve the basic understanding of the physics of high-altitude nuclear detonations by measuring the thermal radiation from the high-altitude Shots Yucca, Orange, and Teak. Spectral irradiances (H_λ) obtained by distant airborne instrumentation are presented as a function of time in four wavelength bands: 0.3μ to 0.4μ, 0.4μ to 0.5μ, 0.5μ to 1μ, and 0.3μ to 3.6μ. The measurements are extrapolated to an assumed point source, and these generalized results are discussed.

Shot Yucca, a balloonborne device detonated at 84,680 feet, radiated approximately like a black body, and, as expected, the thermal pulse had the characteristic shape of a sea level burst. Time to first maximum was approximately time to minimum was , and time to second maximum was The thermal pulse was of shorter duration than a similar low-altitude burst although the total thermal energy was about the same — 40 percent of the device yield.

Shot Orange, a device carried to 140,990 feet by a Redstone rocket, showed marked deviations from low-altitude bursts. Time to first maximum was , the minimum, which was evident only in the 0.5μ to 1μ region, occurred at about ; and the primary thermal pulse was over in . There was a shift in the spectral distribution toward the infrared. In the 0.3μ to 1μ region the total thermal energy was 20 percent of the yield whereas an extrapolated figure for the 0.3μ to 3.6μ region was 45 percent of the yield.

Shot Teak, a device carried to 250,380 feet by a Redstone rocket, had only one thermal maximum occurring at The pulse then decayed The power radiated at maximum, extrapolated to a point source, had a spectral distribution as follows: 0.3μ to 0.4μ, 0.4μ to 0.5μ, 0.5μ to 1μ and 0.3μ to 3.6μ, By subtraction, an upper bound of watts radiated at wavelengths greater than 1μ is obtained. The pronounced shift of the radiation toward the infrared is apparent.

Simple scaling laws are not sufficient to predict the thermal radiation from a high-altitude nuclear detonation. In particular the power radiated in the infrared exceeds by a large factor that expected from a black body of dimensions comparable with the visible fireball. This implies the existence of some mechanism that is producing a greater proportion of infrared radiation than would be obtained using the equilibrium black body theory.

FOREWORD

This report presents the final results of one of the projects participating in the military-effect programs of Operation Hardtack. Overall information about this and the other military-effect projects can be obtained from ITR—1660, the "Summary Report of the Commander, Task Unit 3." This technical summary includes: (1) tables listing each detonation with its yield, type, environment, meteorological conditions, etc.; (2) maps showing shot locations; (3) discussions of results by programs; (4) summaries of objectives, procedures, results, etc., for all projects; and (5) a listing of project reports for the military-effect programs.

PREFACE

Project 8.2 was a large operation with important contributions from many people. The particular efforts of a few are hereby gratefully acknowledged.

The effort and talents of Major Leon Stone, USAF, were primary reasons that this project was so successful. He coordinated and managed the early phases of this work and smoothed the way so well, both in the laboratory and in the field, that the technical work was accomplished in the shortest possible time. He seemed to find solutions where none existed and, in general, efficiently expedited the whole program.

1/Lt. John W. Reed, USAF, was a valuable assistant during and since the Hickam AFB phase and was materially responsible for obtaining the data on Shot Orange by flying as the technical operator on Aircraft RB36-750. This proved to be invaluable since Aircraft RB36-748 failed to obtain data on both Orange and Teak primarily because a civilian scientist was not allowed to be aboard.

J. W. Grenier capably participated in all phases of the operation and was of particular help with the instrumentation and cinespectroscopy. Preshot theoretical predictions were provided by H. K. Sen and A. W. Guess. V. A. Marcello and D. E. Thomas were able assistants during the field operations as were the field crew of the Cook Research Laboratories, in particular E. Rosiak. Thomas B. Smith of Allied Research Associates, Inc., performed an exceptionally capable job in preparing the balloonborne instrumentation and meeting an extremely difficult deadline. Many consultations with I. Kofsky, Technical Operations, Inc., provided understanding and constructive criticism.

The aid of R. E. Pierce, who contributed to the data reduction and preparation of this report, and Louise Mercier, who laid out the graph formats and typed the manuscript, is acknowledged.

Finally, the considerable consultations and advice of M. Annis of American Science and Engineering, Inc., who helped point out the important conclusions of this work, and, in general, the fine support tendered by this group is gratefully acknowledged.

CONTENTS

TABLES

FIGURES

Chapter 1

INTRODUCTION

1.1 OBJECTIVE

The objective was to provide a basic understanding of the thermal radiation resulting from the detonation of nuclear devices at high altitudes. Such an understanding is vital to the evaluation of nuclear weapon effects at high altitudes as applied to such problems as ICBM kill and countermeasures, and, in general, to our defensive retaliatory capability.

Absolute spectral irradiances were to be obtained. For the purpose of this report, thermal radiation has been defined as that radiation extending in wavelength from 1,860 A through the infrared that escapes to large distances from the device. It was necessary to obtain the measurements with sufficient wavelength and time resolution to monitor expected variations in the spectral distribution and intensity as compared to sea level bursts.

Analysis of this data would also aid in understanding the effect of reduced density and different composition of the ambient air at high altitudes.

1.2 BACKGROUND

Although thermal radiation from near sea level nuclear detonations has been well documented, high-altitude bursts were expected to present many new and intricate facets. These arose from changes in two important parameters: (1) the decrease in the ambient air density with the associated changes in collision, attachment, and recombination times; and (2) the change in the composition of the air. New scaling laws were developed that modified the usual hydrodynamic scaling laws by the inclusion of radiation effects, but those too became inoperative with large changes in atmospheric density and composition.

The high-altitude 3-kt burst of Operation Teapot was the only previous applicable experiment, and few significant changes occurred at the moderate altitude (~32,580 feet). It became apparent, however, that most of the thermal energy would be emitted faster at higher altitudes and would have different characteristics. These differences would prove quite important, since the amount of energy, its rate of delivery, and the spectral distribution determine the thermal lethal envelope for missiles and high flying aircraft. The Thermal Radiation Laboratory, Air Force Cambridge Research Center, proposed to obtain the necessary measurements during Operation Hardtack, both with balloon dragline instrumentation and instrumented aircraft.

Originally, the only high-altitude experiment planned was Shot Yucca, a balloonborne device with an expected detonation altitude of 92,000 feet. Later planning included devices to be carried aloft to high altitudes by Redstone rockets: one shot to be detonated at 125,000 feet (Shot Orange) and the other to be detonated at 250,000 feet (Shot Teak).

Since the change in environment was so important to the phenomenology of these bursts, information on the actual yields, heights, times, relative aircraft positions, and some of the associated geophysical parameters (Reference 1) is given in Table 1.1.

1.3 THEORY

Theoretical investigations of nuclear bursts at high altitudes have been carried out by a number of workers (References 2 through 11). The phenomena proved to be extremely complicated with large differences occurring for relatively small variations in yield and altitude in the vicinity of 100,000 feet and higher. One of the primary factors affecting the thermal radiation was the opacity of the fireball. The fireball was still expected to be quite opaque for moderate altitudes (less than 100,000 feet) and to radiate like a black body; however, at much higher altitudes it has a more transparent history and theoretical predictions were more uncertain.

1.3.1 Shot Yucca. The usual hydrodynamic calculations for strong shocks were expected to be applicable to at least 100,000 feet if radiation effects—radiation pressure, energy density, and radiative diffusion—were properly taken into account, that is, if the Rankine-Hugoniot conditions were modified by including the radiation field. Then, as long as the mean free paths of the thermal radiation were small compared with the dimensions of the shock front, the surface of the fireball would radiate like a black body (the opacity of the air preheated by the shock precursor was ignored). These hydrodynamic computations would give the early time history of the radius of the shock front R_s and its temperature T_s. The amount of energy radiated per square centimeter would be $f(T_s)\,\sigma\,T_s^4$ where $\sigma = 5.6724 \times 10^{-12}$ watts/(cm^2 – K^4) and $f(T_s)$ = the fraction of the radiation emitted at wavelengths greater than 1,860 A. Therefore, the radiation rate P from the fireball could be calculated from $P = 4\pi R_s^2 f(T_s)\,\sigma\,T_s^4$. In general the thermal pulse was predicted to be delivered faster than from bursts at lower altitudes. One difficulty in experimental planning for Yucca, however, was that these detailed theoretical calculations were not available before the burst.

Radiation of wavelengths less than 1,860 A does not escape the shock front because of the opacity of cold air, and therefore, only wavelengths greater than 1,860 A would be received at a distant point. In practice, wavelengths shorter than 3,000 A have not been detected at distant stations because of absorption in the ultraviolet, by several ions and compounds, including ozone.

Near sea level, ozone presumably is formed far from the burst very rapidly by the prompt nuclear radiations. This ozone absorbs ultraviolet radiation (2,000 to 3,000 A) very strongly and forms an ultraviolet thermal shield. At higher altitudes the formation of ozone is much slower because of decreased ambient density (three body processes required for ozone formation); consequently, it is expected that the ultraviolet radiation from the burst reaches longer distances. For instance, above 50,000 feet the mean time for formation of ozone is greater than 5 msec, and these times become important, because an appreciable percentage of the thermal energy is delivered by these high-altitude bursts in comparable times. However, the natural ozone layer, which is centered around 90,000 feet, also must be considered.

No theoretical treatment of thermal radiation after breakaway for a detonation near 100,000 feet has been published. Some early estimates were made concerning this late thermal pulse (References 5 and 8), and these will be presented for comparison with the experimental data in Chapter 4. The opacity of a fireball at moderate altitudes was assumed to be rather large throughout the time history; therefore, black body characteristics

were assumed even at late times. The distribution of energy from a black body radiator into each of the wavelength regions of interest to the experimental program is presented as a function of a temperature in Table 1.2 (Reference 12).

1.3.2 Shot Orange. At an altitude of 140,990 feet (actual altitude for Shot Orange) the mean free path of the thermal radiation in the fireball is not always short in comparison to the fireball dimensions and, therefore, the fireball may not always radiate as a black body. As the fireball becomes more transparent, the absorption and emission coefficients of the fireball constituents become increasingly important. The primary processes that must be considered in calculating the opacity of the fireball are the bound-free and free-free transitions and, of lesser importance, bound-bound transitions and electron scattering. (A bound-free transition represents a change from (or to) a discrete energy state to (from) a continuum level—photoionization for example. Thus, bound-bound represents a transition between two discrete levels and free-free between two states of the continuous spectrum.)

At early times the phenomenology of the fireball for Shot Orange was qualitatively similar to that for a sea level detonation. There was an initial phase during which energy transport was principally due to radiation diffusion and a later phase when hydrodynamics (the formation of a strong shock) was the major mechanism for transporting energy. The shock wave formed at a much larger radius than it would at sea level, and the peak temperature of this strong shock was lower than it would be for a sea level burst of the same yield.

During the period prior to breakaway, the mean free path of the thermal radiation within the fireball was short compared with the diameter. Thus, the source of the thermal radiation was relatively opaque, and the early radiation that was measured was related to that from a black body with two exceptions: first, of course, is the absorption by the air that is heated by the precursor; second, is the effect of the nuclear radiations on the total absorption coefficient of the cold air surrounding the fireball. At later times the Orange fireball was expected to be quite transparent. Thus, the radiation time for this fireball was expected to be quite long, and the spectral distribution of this late radiation was not expected to be that of a black body. Rather it was expected to be closely related to the opacity of the air at the temperature in question.

1.3.3 Shot Teak. At an altitude of 250,380 feet (altitude of Shot Teak) the initial mechanism of energy transport was qualitatively different from the dominant mechanisms for the two other detonations. The major fraction of the radiation emitted by the weapon case was deposited within a distance of the order of 3 km from the burst. It was expected that approximately 75 percent of the total yield would be radiated as soft X-rays, and 85 percent of this X-ray energy would then be deposited in a sphere 6 km in diameter within a time determined mainly by the velocity of light. Following this X-ray deposition phase, a radiation diffusion phase occurred, also with great rapidity, and an isothermal sphere was formed approximately 15 km in diameter within a time again determined principally by the velocity of light. The density at the altitude of Shot Teak was so low that it was expected that the fireball immediately following the first phases just described would be quite transparent. Thus, the Shot Teak thermal radiation was not expected to be black body radiation for any appreciable time during its history. The hydrodynamic phase for Shot Teak did not occur Thus, hydrodynamic motions are not of interest during most of the times covered by the thermal measurements. The radiation emitted by the fireball was, as in Shot Orange, modified by the surrounding cold air, which had been sensitized by the nuclear radiation from the

fission products, and in this instance, by the more penetrating thermal X-rays from the case.

During late times when the temperature of the Teak fireball had fallen to approximately 1 volt, the fireball was predicted to become even more transparent. Thus, the time of the thermal pulse for Shot Teak was predicted to be extremely long—of the order of many seconds.

TABLE 1.1 HIGH-ALTITUDE BURSTS AND RELATIVE AIRCRAFT POSITIONS

Shot	Yield	Altitude		P/P_0*	ρ/ρ_0†	Date, Johnston Island Time	Aircraft Position	
							Altitude	Slant Range
		km	ft					
Yucca		25.81	84,680	2.21 (−2)‡	2.91 (−2)	28 Apr 1440	11.3	24.5
Orange		42.97	140,990	2.03 (−3)	2.17 (−3)	11 Aug 2330	9.3	138
Teak		76.31	250,380	2.02 (−5)	3.20 (−5)	31 Jul 2350	9.3	137

* P_0 = 101,325 newtons/m^2.
† ρ_0 = 1.225 kg/m^3.
‡ Number in parentheses indicate the power of 10 by which each entry must be multiplied.

TABLE 1.2 PERCENTAGES OF TOTAL ENERGY RADIATED IN VARIOUS SPECTRAL REGIONS BY A PLANCKIAN RADIATOR AT DIFFERENT TEMPERATURES

Black Body Temperature	Far Ultraviolet (FUV) 0.2μ to 0.25μ	Near Ultraviolet* (NUV) 0.3μ to 0.4μ	Visible (VIS) 0.4μ to 0.5μ	Infrared (IR) 0.5μ to 1μ	Bolometer† (BOLO) λ > 1μ
°K					
1,000	—	—	—	0.035	35.
2,000	—	—	0.03	7.	69.
3,000	—	0.2	1.	27.	62.
4,000	0.03	1.8	5.	42.	47.
5,000	0.3	5.7	10.	47.	28.5
6,000	1	11.	13.	47.	24.
7,000	3	15.	16.	42.	16.5
8,000	5.	18.	16.	38.	13.
9,000	8.	21.	16.	32.	10.
10,000	10.5	21.0	15.2	27.5	8.0
11,000	11.5	20.9	13.9	23.9	6.7
12,000	13.3	20.4	13.0	20.8	5.4
13,000	14.6	19.3	11.8	17.7	4.1
14,000	15.6	18.0	10.8	15.4	3.4
15,000	16.0	17.1	9.7	13.3	3.1
20,000	15.3	11.7	5.8	7.1	1.3
25,000	12.5	7.6	3.5	4.3	0.74

* Experimentally, it was known that no radiation of wavelengths 0.25μ to 0.3μ reached the aircraft.
† The bolometer wavelength band was limited only by the transmission of quartz, ~80 percent from 0.2μ to 2.64μ and from 2.9μ to 3.6μ. The percentages presented are for energies at longer wavelengths than detectable by the dispersion units; λ > 1μ.

Chapter 2

PROCEDURE

2.1 OPERATIONS

The desired measurements of the thermal radiation from high-altitude nuclear bursts required the development of a complex system of airborne instrumentation. The long optical paths through variably absorbing and scattering atmospheres ruled out the location of thermal detectors on the ground or aboard ship.

Two RB-36 aircraft were chosen to carry thermal detection equipment above possible cloud cover and as close to the burst as feasible. It was planned to operate these aircraft at an altitude between 30,000 and 40,000 feet. Special thermal sensors, together with the necessary recording systems, were developed and integrated into an automatic airborne data-gathering system. Each aircraft carried a complete set of instrumentation, which provided the necessary backup and allowed the coverage of a wide dynamic range of possible radiation magnitudes.

Because Yucca was a balloonborne event, it became feasible to locate additional thermal detectors on an instrumentation dragline. With a proposed detonation altitude of 90,000 feet, there would still be at least 70 percent of the atmospheric ozone between the aircraft and the nuclear device. The attenuating effects of ozone are particularly strong in the ultraviolet region, and thus, aircraft measurements in this region would be obscured. Accordingly, thermal detection, calibration, and delayed telemetry systems were installed in canisters on the dragline configuration of the balloon. Three thermal canister stations were located at various distances below the device to obtain attenuation measurements as well as provide the backup and dynamic range so necessary for securing data from such one-shot thermal events.

2.1.1 Shot Participation. The project participated in Shots Yucca, Orange, and Teak (Table 1.1). The nuclear device for Shot Yucca was suspended from a free balloon. The balloon was launched from the deck of the aircraft carrier USS Boxer. Shots Orange and Teak were thermonuclear devices carried aloft by rocket vehicles launched from Johnston Island.

2.1.2 Pretest Activities. Aircraft and canister systems development and installation had been essentially completed prior to departure for the forward test area. In the field, many checks and dry runs were conducted to insure that operation of the complex aircraft and canister instrumentation was satisfactory. These checks included the recording and playback of simulated thermal pulses over each of the many detection and recording channels.

After final estimates of the detonation point and aircraft positions were made available by Joint Task Force 7 (JTF-7), the anticipated ranges of flux levels were computed for each thermal detector at each of the various locations, allowing for final system sensitivity level adjustments. Prior to each shot, preflight checks were accomplished; these consisted of detector calibrations, sensitivity adjustments, recorder erase and alinements,

system calibrations, logic functions, camera loading and calibrations, and system performances. Manual in-flight checks and monitoring of automatic instrumentation sequencing was based on the broadcast event countdown.

2.2 INSTRUMENTATION

To accomplish the close-in thermal measurements on Shot Yucca, a remotely controlled thermal detection and delayed telemetry system was installed in each of three canisters. These canisters were suspended on the balloon dragline at positions 1,050, 1,500, and 2,100 feet below the nuclear device. Each canister was equipped with a set of spectroscopic detectors, a multichannel magnetic tape record and playback system, a command receiver, and a telemetry transmitter, together with sufficient battery power. Space and instrumentation in each canister were shared with Project 1.10 for pressure measurements. Command and telemetry links were established between each canister and a control station on the USS Boxer. Figure 2.1 illustrates the balloon and dragline configuration. A typical thermal and pressure canister internal assembly is shown in Figure 2.2, and a block diagram of the thermal instrumentation contained by each is given in Figure 2.3.

The two RB-36 aircraft were employed as instrumentation platforms for the relatively distant thermal measurements of all three events. The various electrical and photographic thermal detectors were mounted behind specially constructed optical windows installed in the fuselage of each aircraft. Aircraft instrumentation space and control circuitry were shared with other projects. The thermal instrumentation in each aircraft consisted of spectroscopic detectors, automatic sequencing and calibration logic, multichannel magnetic-tape recorders, spectroscopic cameras, and a command receiver, together with the necessary power supplies and control circuitry. The system functioned automatically upon reception of command signals over a radio link from the control center at the launching site on the USS Boxer or at Johnston Island. The detection and recording system is outlined in the block diagram of Figure 2.4.

2.2.1 Thermal Detectors. Both the aircraft and the canisters were equipped with broadband spectroscopic detectors (Figures 2.5 and 2.6) developed by the Thermal Radiation Laboratory, Air Force Cambridge Research Center (AFCRC), under contracts with Paul M. McPherson Precision Instruments and Allen B. DuMont Laboratories, Inc. (Reference 13). These sensors were designed particularly for the measurement of irradiance as a function of time and wavelength at high altitudes. Unique sensors were required, because standard radiometers and calorimeters did not have sufficiently fast time responses or spectral definition. Response time was of particular importance in these events, because the thermal pulse was expected to be delivered much faster than for sea level bursts.

Four separate instruments were designed, each sensitive to a portion of the electromagnetic spectrum between 2,000 and 10,000 A (Table. 1.2). These detectors, each designed to have a flat wavelength response within its spectral range, were named dispersion units.

The dispersion unit was basically a standard dispersive system utilizing slit, collimating lens, prism, focusing lens, and multiplier phototube detectors. The unique facets of its design were the special prism and the focal plane mask (Figures 2.5 and 2.6). A straight-through design was achieved using a one-piece, six-sided Mertz prism. The use of an optical mask in the focal plane provided sharp cutoffs and flat response with respect to wavelength. The mask aperture was essentially the mirror image of the detector response versus wavelength. The response versus wavelength of the various units was not as flat as desired because of the short time available for instrument development.

Each of the dispersion units employed two roughened quartz diffusion disks in front of the slit to provide a wider field of view and reduce pointing error. Figure 2.7 shows the field of view thus obtained and compares it with the field of view of the same instrument using a clear window. The double diffusion disks caused a loss factor of about 30 in sensitivity and also affected the shape of the mask aperture, because the diffusing (scattering) was wavelength dependent.

Each spectral region required an instrument with different slit widths, lens focal lengths, prism designs, and photocathodes. Quartz prisms were used in the FUV and NUV dispersion units. Special crown and dense flint glass, developed by Bausch and Lomb Optical Co., was used in the VIS and IR units located on the balloon dragline. This glass was particularly resistant to change under high neutron and gamma irradiations (Reference 14). Spectrally selective photocathode materials were chosen for each wavelength region. The 3/4-inch phototubes were designed and connected for use either as photomultipliers at 1,000 volts or as simple photodiodes at 300 volts, depending upon the required sensitivity.

In addition to the dispersion unit configurations, the aircraft were equipped with a fast response bolometer and a calorimeter, and the canisters were equippped with a radiometer. These instruments were black body type detectors whose spectral response was limited only by the quartz windows protecting the instrument faces.

The bolometer was designed for the Thermal Radiation Laboratory by the Allied Research Associates, Inc., to measure total irradiance as a function of time (Reference 15). This unit consisted essentially of a resistance bridge circuit, one arm of which changed according to the magnitude of the thermal flux incident upon it.

The radiometers and calorimeters were supplied by the Naval Radiological Defense Laboratory (NRDL). These were thermocouple-junction detectors; the radiometer measured total irradiance as a function of time, while the 20-junction calorimeter measured total energy (Reference 16).

All thermal detectors in the aircraft were located behind glass or fused silica (quartz) windows. Transmission characteristics of the glass are presented in Figure 2.8 and of the fused silica in Figure 2.9. A diagram of the instrument arrangement behind the aircraft windows is shown in Figure 2.10, and the actual windows and detectors are shown in Figures 2.11 and 2.12.

2.2.2 Recording Systems. The requirements for recording systems differed considerably between the aircraft and dragline canister thermal detection systems. Because of space, weight, and power limitations, only a relatively small number of detectors could be installed in each canister, requiring a small recorder with several channels. In addition, since the canisters would not be recoverable, an automatic playback of each recorded channel into the canister telemetry link was required. This delayed telemetry technique was necessary because radio blackout due to ionization of the surrounding atmosphere by the radiations from the burst would likely prevent any direct telemetry of the brief thermal radiation pulse. Also, limited frequency response of the telemetry link required a slower playback speed than during record, to faithfully reproduce the anticipated rapid signal fluctuations. The canister recorder and instrumentation had to survive and function reliably in a high-altitude environment subject to neutron and gamma radiation from the nuclear device. The equipment was also required to operate through accelerations encountered during launch, deployment, blast, and free fall.

Accordingly, a miniaturized canister magnetic tape recorder and playback system was developed under contract with Gulton Industries, Inc., for the joint use of Projects 8.2 (thermal) and 1.10 (pressure). The recorder utilized two 1/4-inch continuous tape loops. One loop was for amplitude modulation recording of six thermal data channels, whereas the

other loop was used for FM recording of pressure measurements. The six channels for the simultaneous recording of the thermal pulse in various wavelength ranges were achieved by positioning three dual-track record heads around a 21-inch magnetic tape loop driven at 7.5 in/sec. Each head recorded for only 240 msec after the burst, after which the record heads were deenergized to prevent any recording overlap on the tape. The first 125 msec of this recording period were for the thermal pulse, and the remaining 115 msec were used for the automatic recording of a 1.5-volt, 400-cps damped sinusoid to establish an amplitude and frequency reference. The canister recorder is shown in Figure 2.13.

Following a 10-minute warmup period, the canister recorder was activated 10 seconds prior to the burst by a VHF command signal from the shipboard telemetry station. During the burst, six channels of thermal data were recorded while simultaneously two of the channels were directly telemetered in the unlikely event that some transmissions might penetrate the ionization blackout. At the conclusion of the record cycle, the recorder automatically switched into the playback mode for repeated playback and telemetry, two channels at a time, throughout the free fall of each canister. The telemetered data was demodulated and recorded at the telemetry station aboard the USS Boxer, using standard multichannel FM recorders. The canister and ground telemetry system was developed, installed, and operated by the Bendix Aviation Corporation.

The less stringent space, weight, power, and environmental requirements within the aircraft allowed the use of a relatively large number of thermal sensors. Each sensor required at least one recording channel, but where available the dynamic range of possible inputs could be increased by a second, parallel recording channel. This wide recording range was necessary because of unknown variations in predicted irradiances. Accordingly, Ampex 800 airborne magnetic tape recorders (Figure 2.14) were employed in each aircraft. These 14-channel (1-inch tape) recorders, when used for FM recording of the thermal pulses, exhibited a frequency response of dc to 10 kc when operated at a tape speed of 60 in/sec. The upper limt was reduced to 5 kc when operated at 30 in/sec.

The signal outputs from the phototube detectors, which ranged from about 0.01 to 10μa, were directed through a console of 14 dc preamplifiers developed by George A. Philbrick Researches, Inc., (Figure 2.15). These chopper-stabilized, operational amplifiers of variable gain converted the signal currents to the voltages and impedances required to drive the Ampex FM record amplifiers. The preamplifiers provided the offset voltages necessary for the utilization of the full dynamic ranges of the recorders and presented low output impedances so that the shunt capacities of the coaxial signal cables to the recorders did not limit the frequency response. An overall system frequency response of approximately dc to 7 kc was achieved. The upper frequency limit was determined primarily by the shunt capacities of the signal cables from the phototubes.

The bolometer was provided with a special ac amplifier, which had a gain variable to 10^5 and a frequency response of 5 to 10,000 cps. The bolometer amplifier and power supply required very low noise characteristics. One of the dc preamplifiers of the Philbrick console was used to amplify the signal from the calorimeter for Shot Yucca; however, it was replaced by an Electro-Mechanical Research operational amplifier for the other shots.

2.2.3 Photographic Detectors. Photographic instrumentation for the recording of thermal data consisted of four N-9 gun-sight-aiming-point (GSAP) 16-mm cameras (Figure 2.16) and one high-speed Traid 16-mm camera in each aircraft. Two of the GSAP cameras were used with spectroscopic film and AFCRC cinespectroscopic nosepieces to record fireball spectra in the wavelength range from 4,000 to 6,200 A, while the other two used microfile film to provide aiming, field of view, and documentary information. All GSAP cameras were operated at 64 frames/sec. The Traid camera was outfitted with a similar

spectroscopic nosepiece but recorded the spectra at 200 frames/sec.

The spectroscopic nosepieces were low resolution ($\Delta \lambda \geq 20$ A) devices that utilized three-element Amici dispersing prisms. Figure 2.16 shows one of the nosepieces attached to a GSAP camera. These instruments are described in detail in Reference 17.

2.2.4 Calibration. The dispersion units were calibrated for absolute sensitivity and wavelength characteristics in the laboratory, utilizing standard sources, calibrated detectors, and a monochrometer. The relative sensitivities between units of the same spectral range were obtained and then rechecked immediately before and after each shot, using an analog flash source (Reference 18). Since the relative sensitivities of the dispersion units were known, two units in each range were calibrated absolutely, and the others were then evaluated relative to these. Sensitivities and wavelength passbands of the units that obtained the best data from the three shots are listed in Tables 2.1 through 2.3. The relative flatness of the response versus wavelength of the various instruments was estimated to be 20 percent, but individual units varied considerably.

Since the detectors could not be aimed precisely, the sensitivity as a function of the pointing error (deviation of line of sight from the optical axis) had to be determined. Typical curves of the fields of view of the NUV, VIS, and IR dispersion units are shown in Figures 2.17 through 2.19. The actual aiming of the aircraft detectors was determined from the GSAP cameras. The small range of pointing error for the dragline canisters was established from many dry runs.

Initial calibrations of the bolometers were made in the field, using at both the Eniwetok Proving Ground (EPG) and Hickam AFB, Hawaii, the zenith sun as the standard source. The maximum possible irradiance value of 100 mw/cm^2 was assumed. Later bolometer calibrations were accomplished in the laboratory, utilizing a standard lamp and light chopper. The sensitivities from the 2 techniques corresponded within 25 percent; however, the bolometers failed internally before the final checks were completed. The calibrations for the calorimeters and radiometers were provided by the manufacturers.

Aircraft system calibration to establish a signal amplitude reference on each data record was accomplished by the automatic substitution of a stepping function of five calibration voltages into each channel in place of the sensor outputs. This was done in the calibration and junction box mounted on the amplifier console in Figure 2.15. The voltage function was sequentially generated, using a timing motor and cam-operated switches. Two cycles of the voltage steps were recorded prior to and also after the nuclear burst. The data-recording period extended from H − 1 minute to H + 1 minute to provide a wide margin for error. The calibration voltages, which were derived from mercury cells and precision resistor divider networks, were accurately measured prior to and after each flight with a Fluke 1801 differential voltmeter.

Amplitude-modulated 60-cps speedlock amplifiers were used with each Ampex magnetic tape recorder to insure that record and playback tape speeds were the same. An additional time reference was established for Shot Orange by recording a precision (0.001 percent) 1-kc sine wave on one channel of each recorder throughout the data-recording time. This was generated by an American Time Products, Inc., temperature compensated tuning fork and amplifier. A separate recording channel was also used to record the countdown, fiducial tones, and aircraft intercom for all three events.

References for magnitude and time were automatically established for the canister data by the 400-cps damped sinusoid, which was sequenced into each channel after the recording of the thermal pulse. This function was accurately calibrated prior to balloon launch.

The spectroscopic film interpretation required the calibration of two variables: the wavelength as a function of the horizontal position on the film surface, and the incident energy

as a function of the density of the exposed film.

The wavelength calibration was obtained by exposing the film, through the mounted nosepieces, to light from a mercury arc lamp immediately before the installation of the camera assembly into the aircraft. The wavelengths of the resulting slit images on film were the well-known mercury lines and could be used to determine a dispersion curve.

The planned calibration of the spectral camera assemblies in terms of incident energy as a function of film density was not satisfactory because of the malfunction of the optical pyrometer in the field. An alternative method of approximate calibration was therefore used. A sensitivity curve (Figure 2.20) for the type of film being analyzed was used as the basic standard. This curve shows the ergs/cm^2 required to produce 0.6 density above the gross fog level of the film. The film was processed by Edgerton, Germeshausen and Grier (EG&G) to give $\gamma = 1$ for D = 2.5, i.e., the ratio of the change in density to the change of logarithmic exposure was unity. These known factors gave an approximate value for the energy incident upon the film surface, which did not take into account several transmission factors, particularly the fact that the transmission of the nosepiece assembly was strongly wavelength dependent.

2.2.5 Data Reduction. Preliminary data reduction in the field was accomplished using a Consolidated Electrodynamics Corporation (CEC) 5-114 recording oscillograph to produce visual records of the thermal pulses and calibration data. An Ampex 300 FM magnetic tape playback system followed by a suitable Philbrick wideband dc high-current amplifier was used to drive the CEC recording galvanometer. The calibration deflections, dispersion unit sensitivities, terminating load resistors, window transmissivities, and sensor pointing errors were all used to determine the calibration constant to apply to the thermal pulse deflections to give absolute values of irradiance as a function of time and wavelength for each shot.

For detailed data reduction in the laboratory, an Epsco timing sequence and buffer storage system (Figure 2.21) was developed specifically for analyzing waveforms characteristic of nuclear thermal pulses. This system permitted the high-speed sampling of analog voltages, converted them into digital code, provided storage and format arrangement of the converted data, and then displayed the data via a Commercial Controls Model 2 paper tape punch. An Ampex FR 100A magnetic tape system was used to play back the data tapes into an Epsco Datrac B6135, which accomplished the analog-to-digital conversion. The system included an input amplifier with gains variable from 1 to 30.

This data reduction system was provided with two modes, for the sampling of both fast and slow rise-time analog voltage waveforms. In the fast mode, signal voltages could be sampled at two independent consecutive rates, to permit the data sampling to automatically fit a particular voltage pulse shape. Sampling rates from 1 to 25 kc were available in this mode with a total number of samples in 1 cycle of 298. In the slow mode of operation the sampling rates available were from 1 to 100 cps.

The 25-kc sampling rate was used on all thermal pulses, providing accurate time measurements to the first peaks as recorded. The combination of the 25-kc sampling rate with a tape playback speed of 30 in/sec gave a time resolution of 20μsec, which exceeded the time resolution of the detector-recorder system (~50μsec). The slow mode of operation was used for the readout of the calibration signals.

The punched paper tape output of the Epsco system was then automatically plotted by a Benson-Lehner electro-plotter for a visual observation of the data conversion. Readout was also possible in printed form, using a Commercial Controls Flexowriter FPC 8-P. The paper tapes were then converted to International Business Machine (IBM) cards, using the IBM-047 converter, for processing by an IBM-650 electronic data-processing machine,

which applied scale correction factors and integrated each pulse to obtain total energy as a function of time. Figure 2.22 shows a block diagram of the data-processing system.

2.2.6 Film Data Reduction. Densitometer traces of the spectrographic film data were obtained by means of a Jarrell-Ash microdensitometer. Only a few representative frames of each film were examined, since a visual scanning of the films indicated no abrupt changes as a function of time. The maximum time resolution of 5 msec was too slow to detect the very early fluctuations. The calibration factors were applied to the traces to give curves of energy at the film surface.

The documentary cameras were alined with the optical axis of all the aircraftborne detectors, and processed films from these cameras were used to compute the deviation from the optical axis of the burst point for each shot.

TABLE 2.1 DETECTORS OBTAINING DATA, SHOT YUCCA

Aircraft Number	Detector		Bandwidth*	Sensitivity	Description of Pulse†	Recording System
			A	amp/(w/cm²)		
50	FUV	89	2,000 to 2,500	510	L	1
50	NUV	2	2,500 to 4,000‡	107	L	1
50	NUV	14	2,500 to 4,000	187	H	2
48	NUV	18	2,500 to 4,000‡	68	L	1
50	VIS	27	4,000 to 5,100	28.5	H	1
50	VIS	31	4,000 to 5,000‡	19.2	H	1
50	VIS	31	4,000 to 5,000‡	19.2	H	2
48	VIS	35	4,000 to 5,000‡	17.2	H	1
48	VIS	43	4,000 to 5,000‡	6.7	L	1
50	VIS	47	4,000 to 5,000‡	10.4	L	1
50	VIS	47	4,000 to 5,000‡	10.4	L	2
48	IR	16	4,700 to 9,700	0.42	H	1
50	IR	28	5,000 to 10,000‡	0.42	L	1
50	IR	40	5,000 to 10,000‡	1.44	L	2
50	IR	44	5,000 to 10,000	0.395	H	1
50	IR	44	5,000 to 10,000	0.395	L	2

* Cutoff wavelengths are chosen at 50-percent sensitivity with the following average error: NUV units 4,000 ± 110 A; VIS units 4,000 ± 40 A, 5,000 ± 65 A, IR units 5,000 ± 200 A, 10,000 ± 340 A.

† L, low signal-to-noise; H, high signal-to-noise.

‡ Exact cutoffs not measured.

TABLE 2.2 DETECTORS OBTAINING DATA, SHOT ORANGE

Aircraft Number	Detector		Bandwidth*	Sensitivity	Description of Pulse†	Recording System
			A	amp/(w/cm²)		
50	FUV	57	2,000 to 2,500	68	L	1
50	FUV	57	2,000 to 2,500	68	H	2
50	NUV	78	2,500 to 4,200	65	L	1
50	VIS	31	4,000 to 5,000‡	19.2	H	1
50	VIS	55	4,000 to 5,000‡	1.3	L	1
50	VIS	55	4,000 to 5,000‡	1.3	H	2
50	IR	12	5,000 to 10,000‡	0.29	L	2
50	IR	16	4,700 to 9,700	0.42	L	2
50	IR	48	5,200 to 10,100	0.157	L	1

* Cutoff wavelengths are chosen at 50-percent sensitivity with the following average error: NUV units 4,000 ± 110 A, VIS units 4,000 ± 40 A, 5,000 ± 65 A, IR units 5,000 ± 200 A, 10,000 ± 340 A.

† L, low signal-to-noise, H, high signal-to-noise.

‡ Exact cutoffs not measured.

TABLE 2.3 DETECTORS OBTAINING DATA, SHOT TEAK

Aircraft Number	Detector		Bandwidth*	Sensitivity	Description of Pulse†	Recording System
			A	amp/(w/cm²)		
50	FUV	57	2,000 to 2,500	68	L	1
50	FUV	57	2,000 to 2,500	68	H	2
50	NUV	78	2,500 to 4,200	0.19	H	1
50	NUV	6	2,500 to 4,100	50	H	1
50	VIS	23	3,960 to 4,980	54	H	1
50	VIS	55	4,000 to 5,000‡	1.3	L	1
50	IR	48	5,200 to 10,100	0.157	H	2
50	IR	56	5,000 to 10,000‡	0.014	H	1

* Cutoff wavelengths are chosen at 50-percent sensitivity with the following average error: NUV units 4,000 ± 110 A; VIS units 4,000 ± 40 A, 5,000 ± 65 A, IR units 5,000 ± 200 A, 10,000 ± 340 A.

† L, low signal-to-noise, H, high signal-to-noise.

‡ Exact cutoffs not measured.

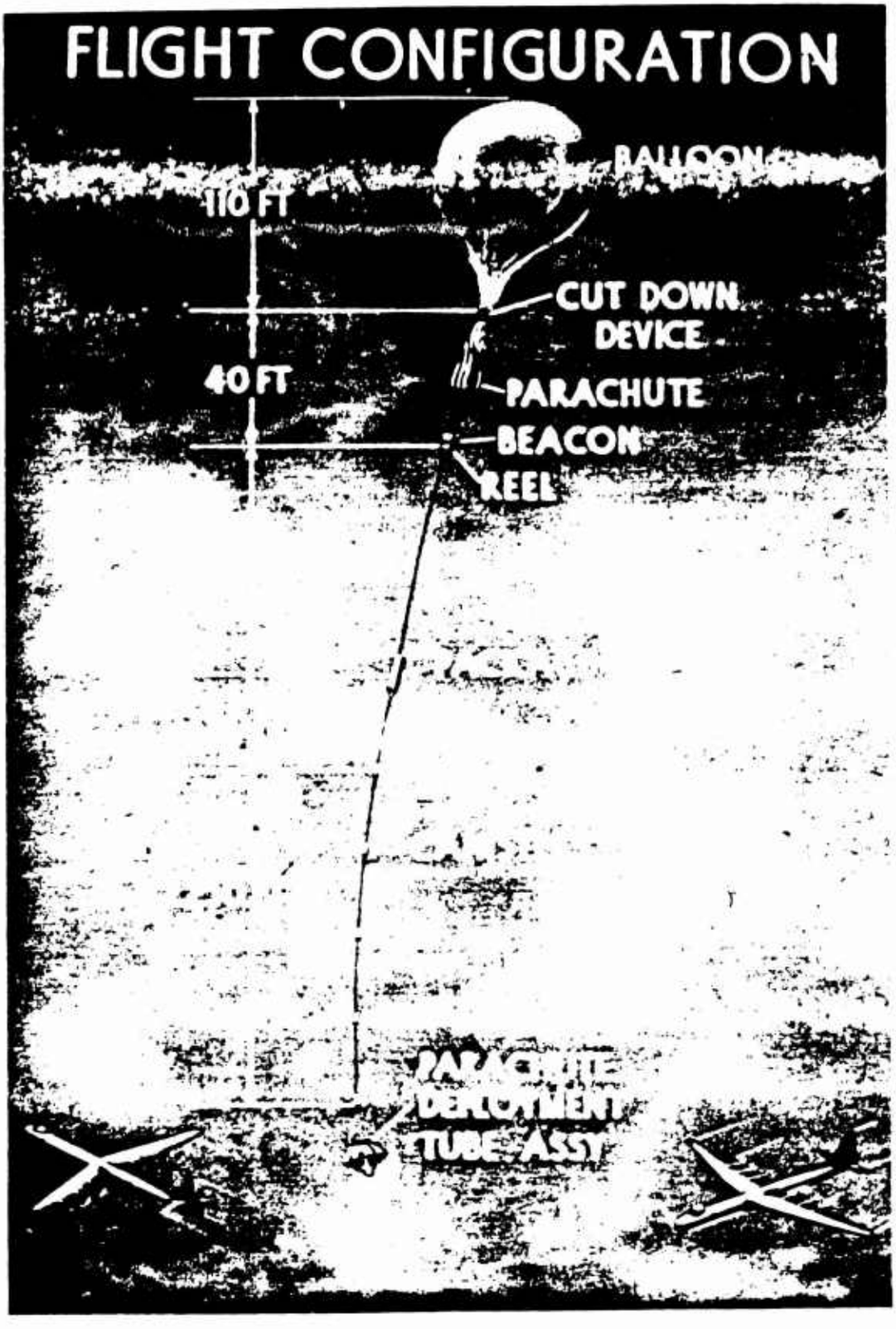

Figure 2.1 Flight configuration illustrating dragline, Shot Yucca.

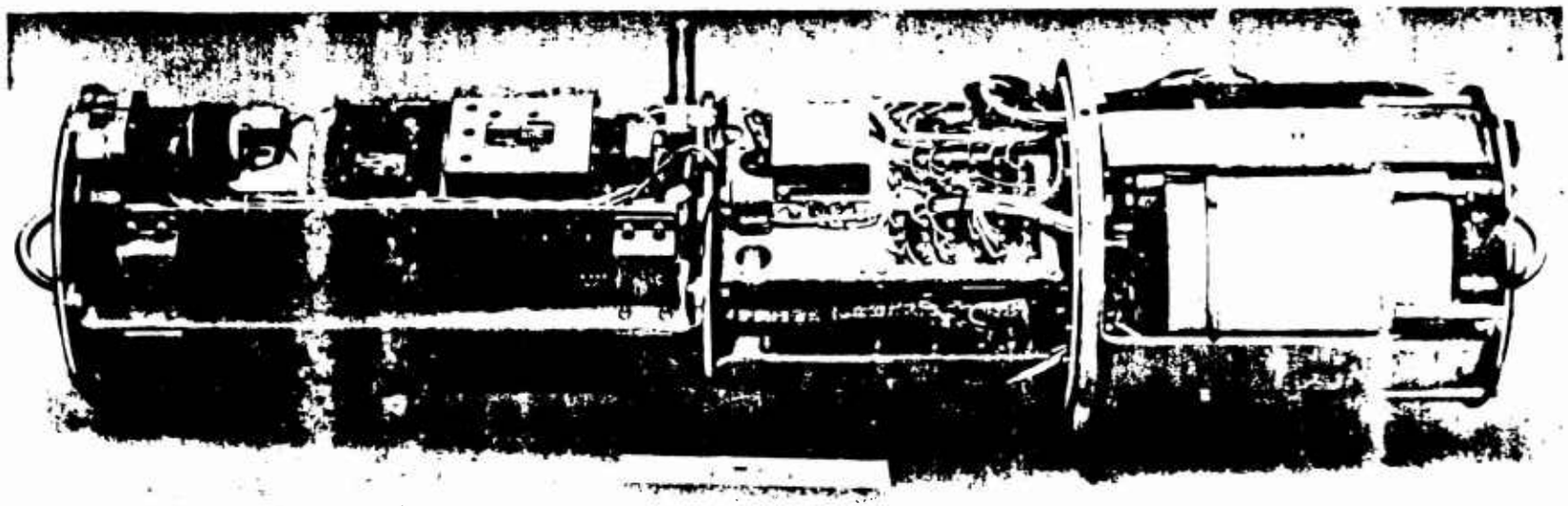

Figure 2.2 Typical thermal and pressure canister, Shot Yucca.

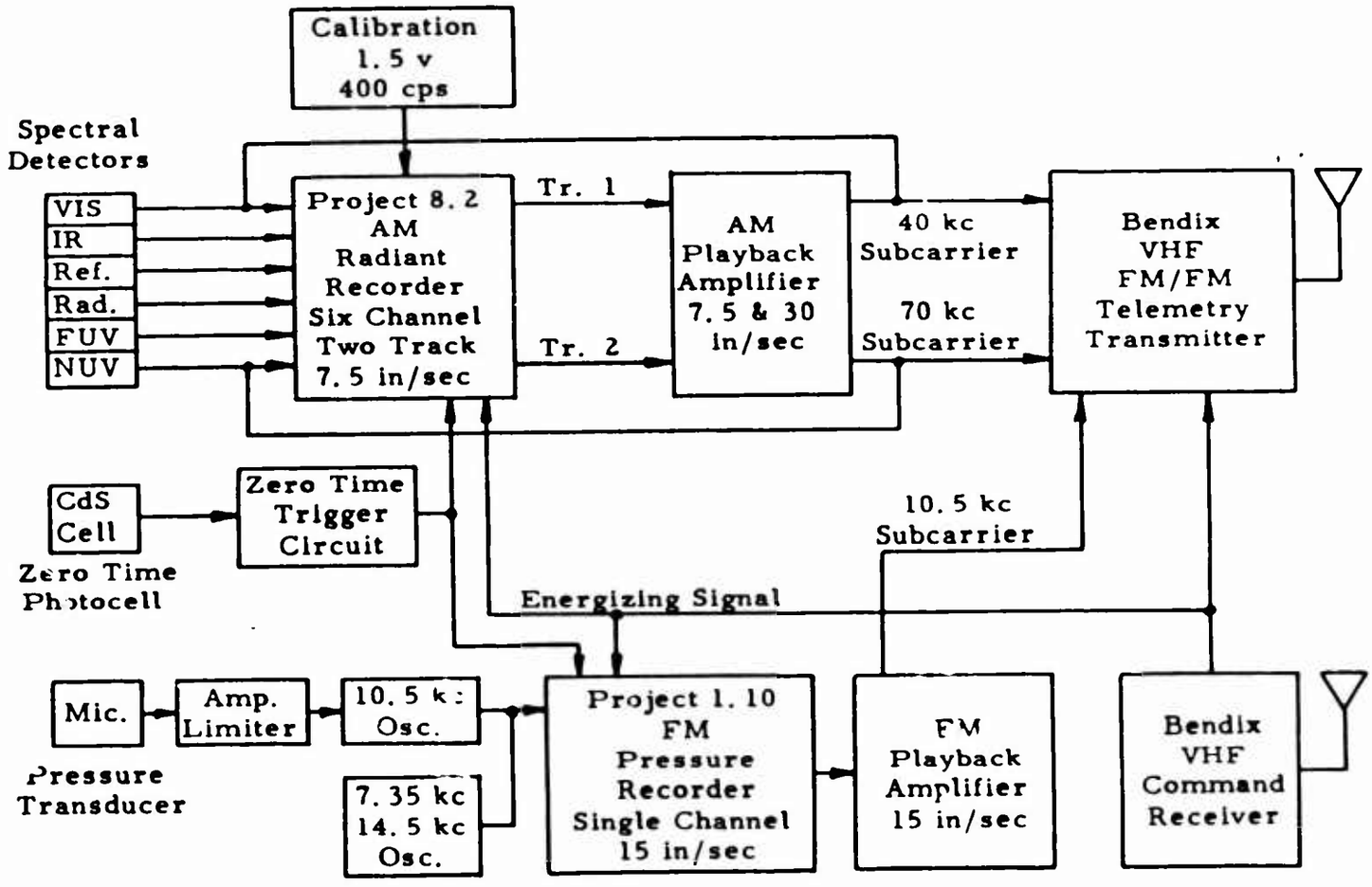

Figure 2.3 Block diagram of thermal dragline instrumentation, Shot Yucca.

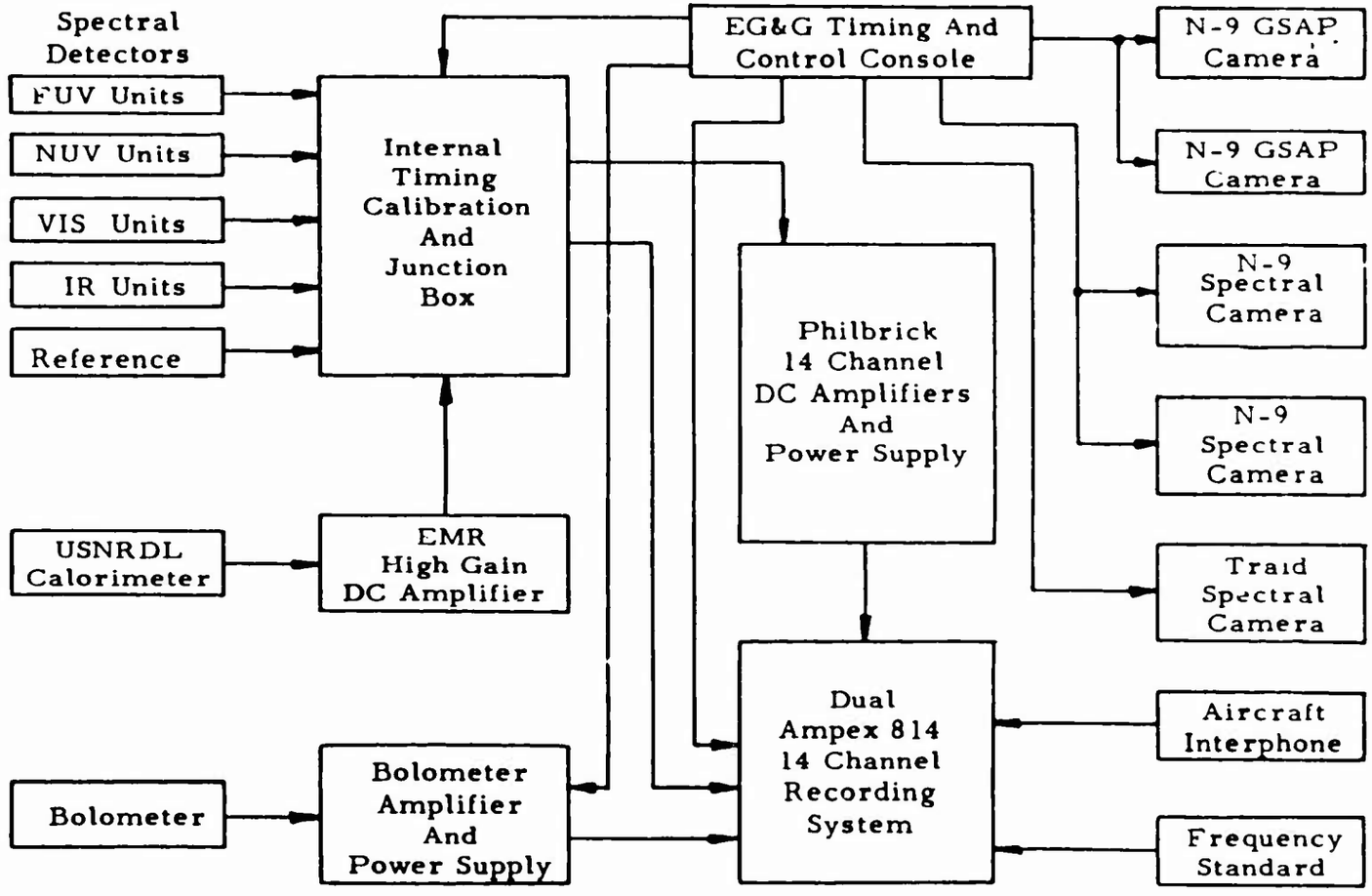

Figure 2.4 Block diagram of thermal aircraft instrumentation.

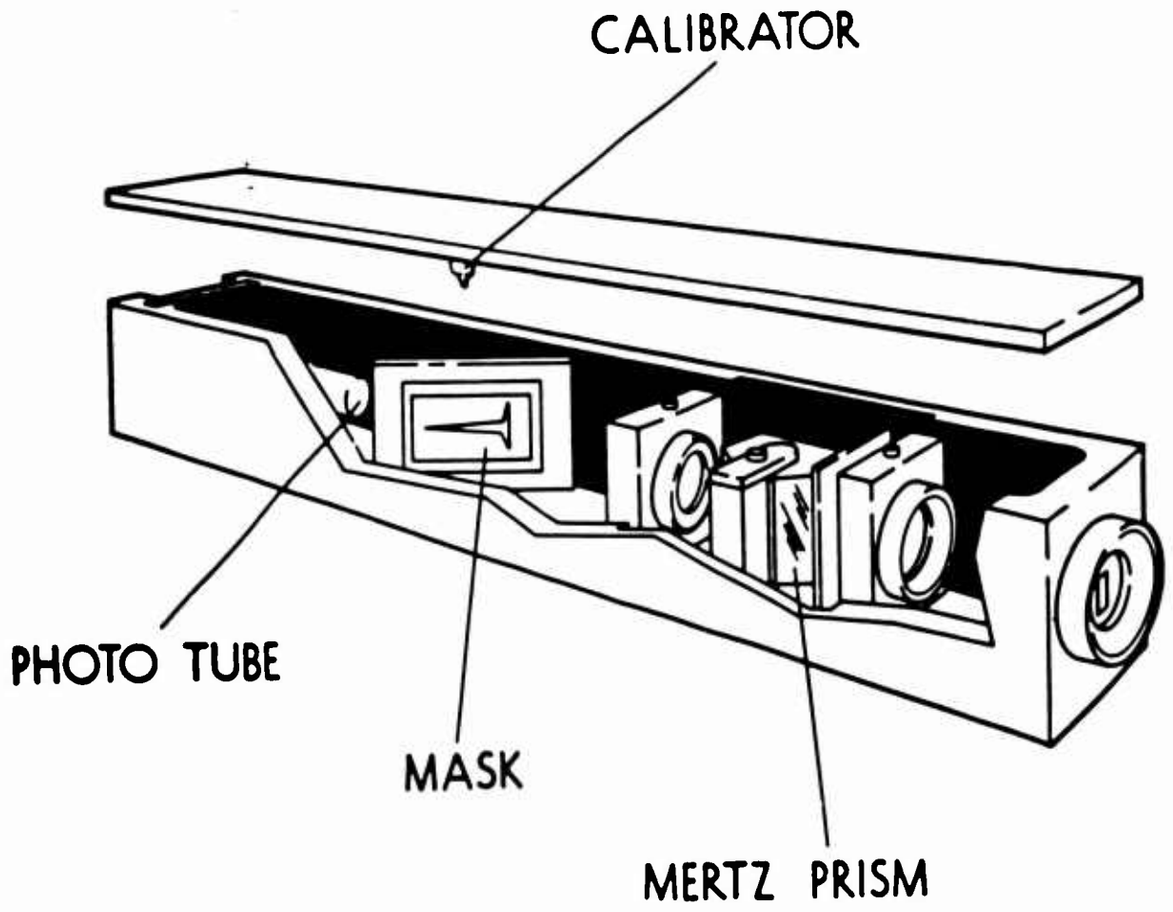

Figure 2.5 Schematic of AFCRC broadband photodetector (dispersion unit).

Figure 2.6 Photograph of a typical dispersion unit.

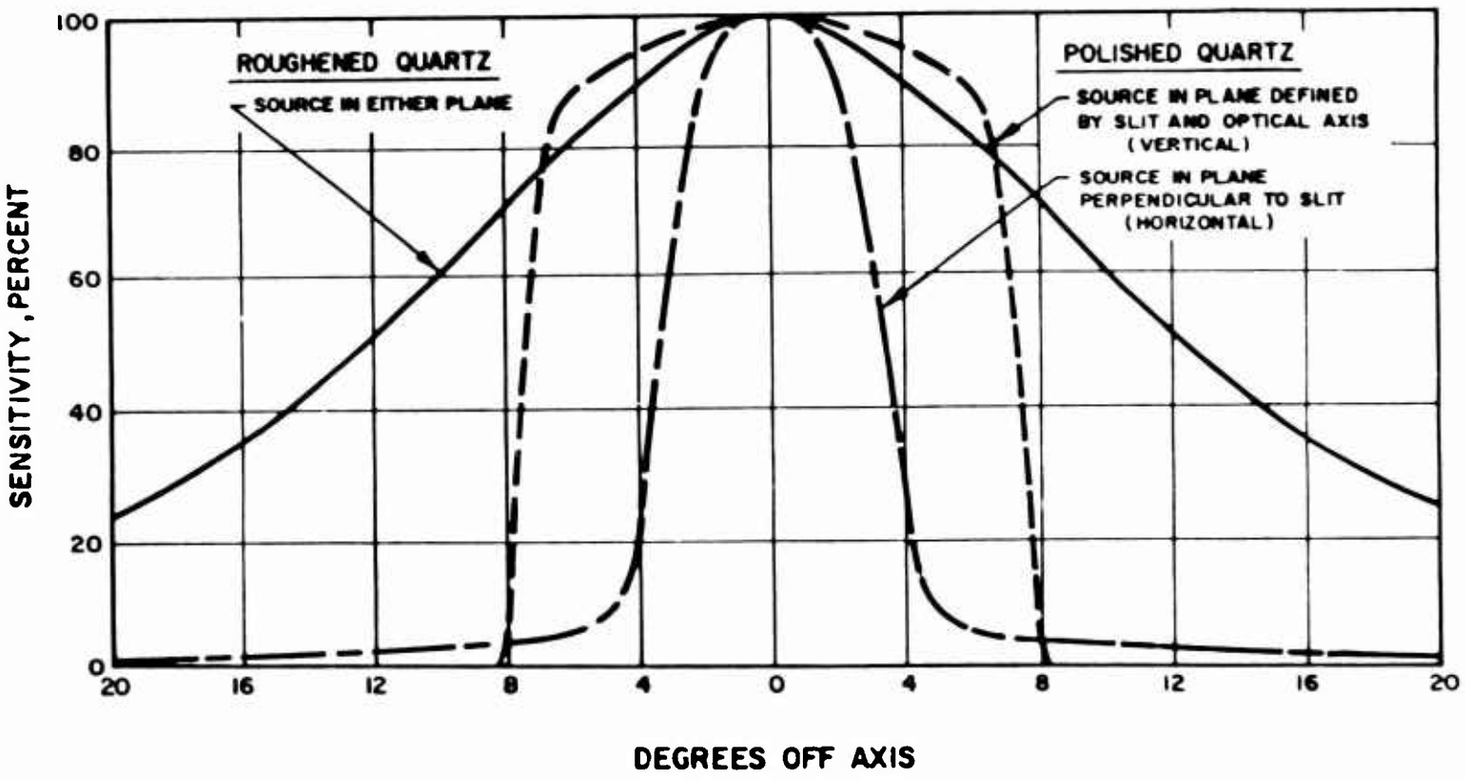

Figure 2.7 Variation in field of view of a typical IR dispersion unit.

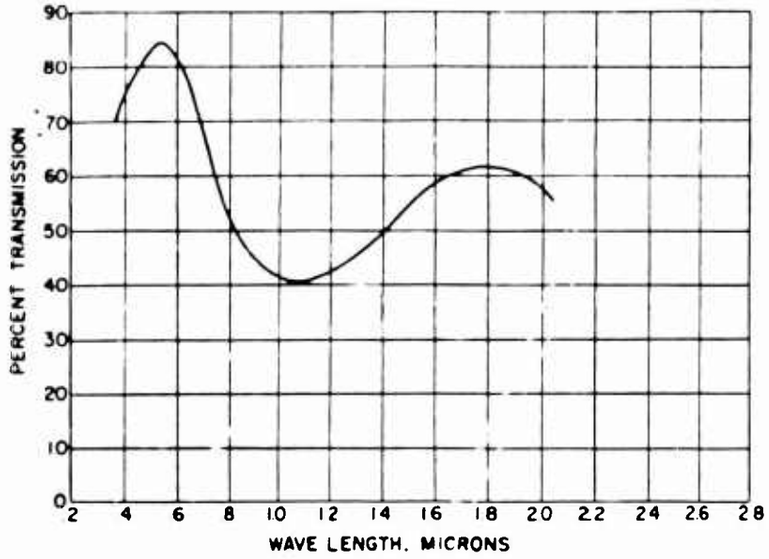

Figure 2.8 Transmissivity of glass used for aircraft windows.

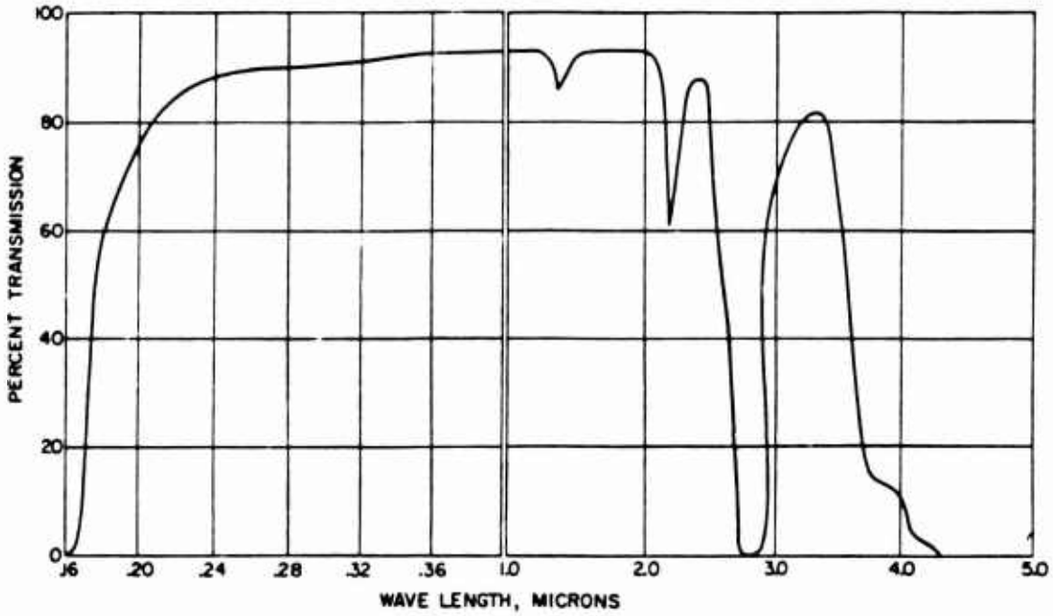

Figure 2.9 Transmissivity of fused silica windows.

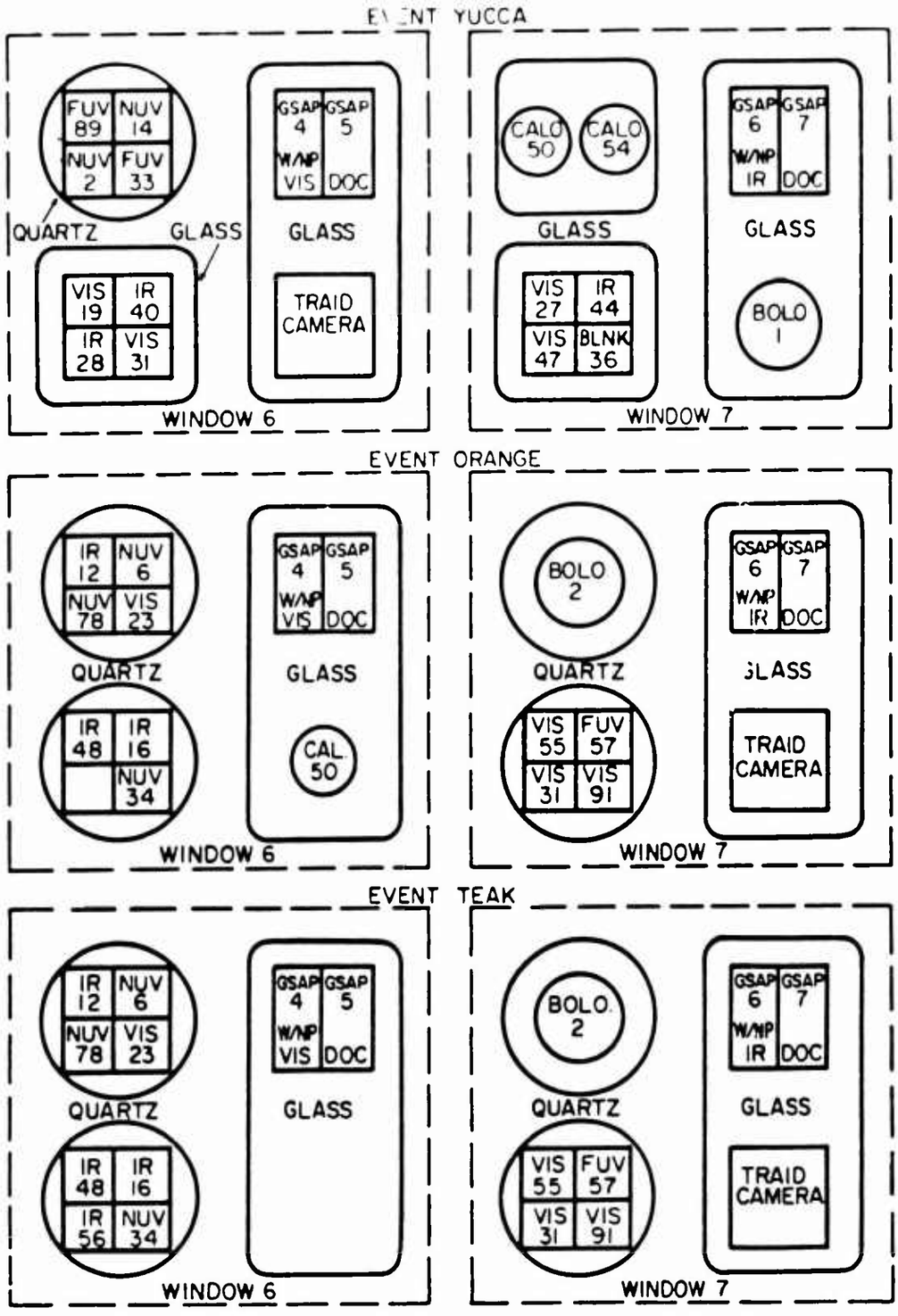

Figure 2.10 Schematic of windows and instrument configuration in aircraft.

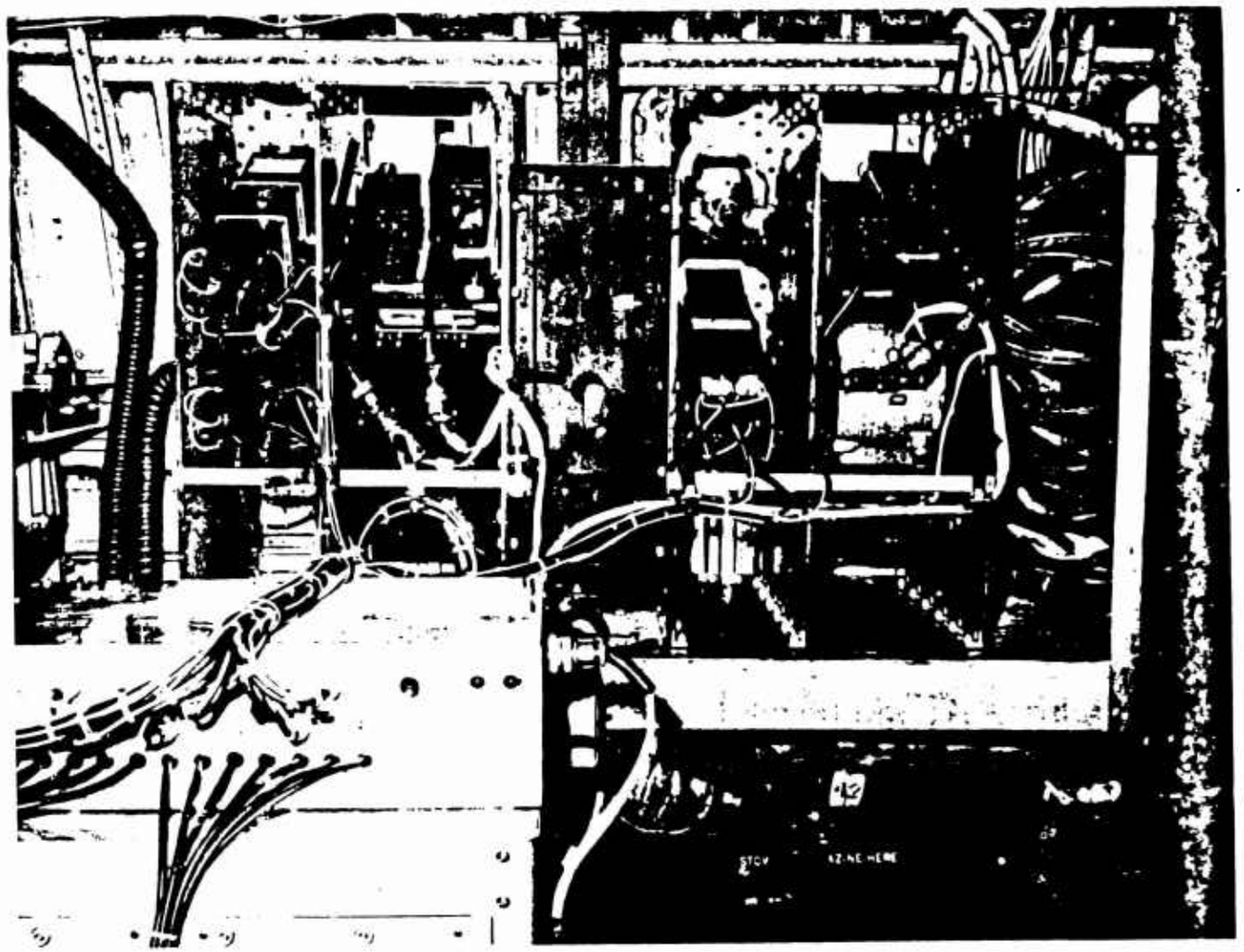

Figure 2.11 Photograph of detectors mounted in aircraft instrumentation compartment.

Figure 2.12 Exterior view of aircraft windows and instrumentation.

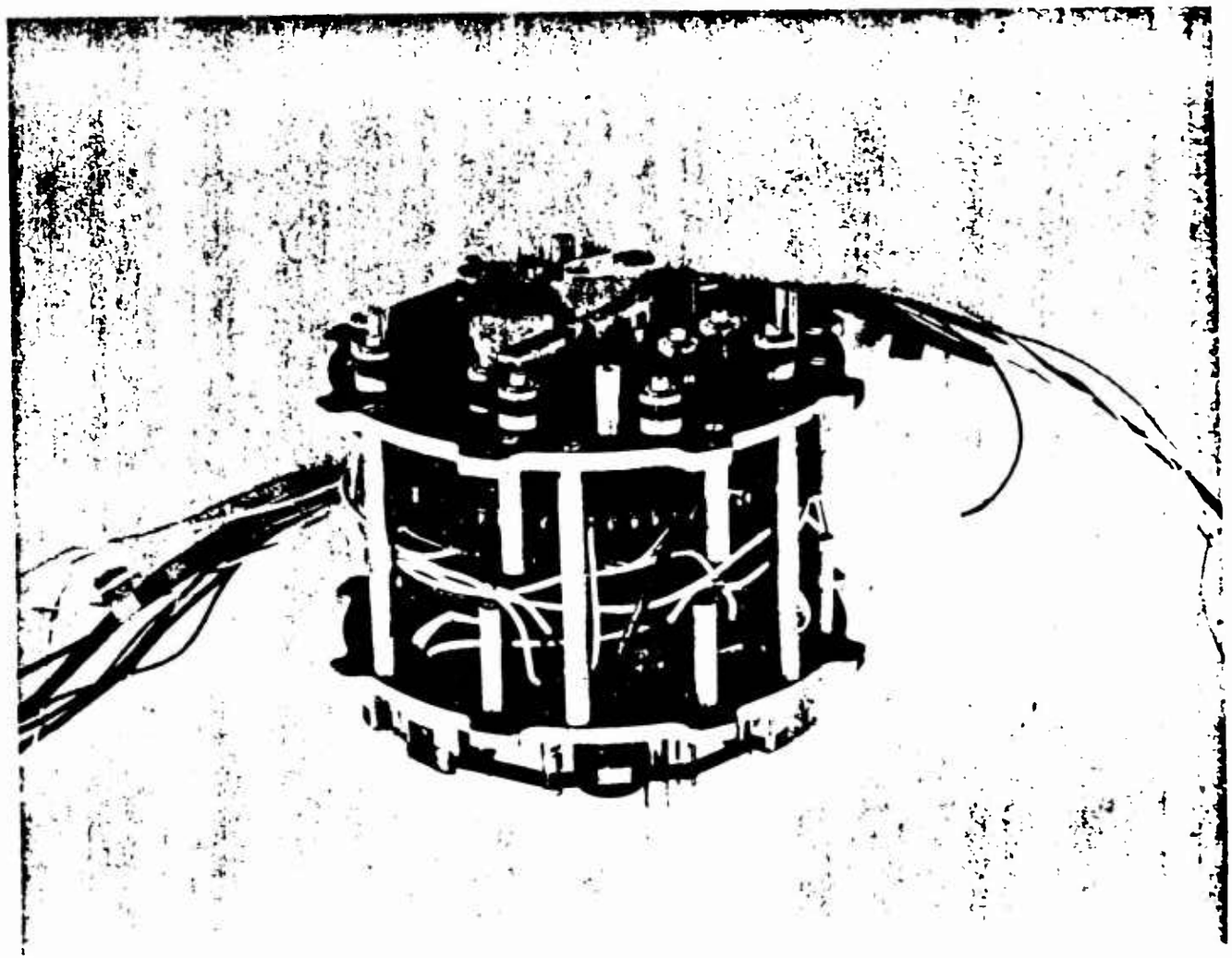

Figure 2.13 Canister magnetic tape recorder for thermal and pressure measurements.

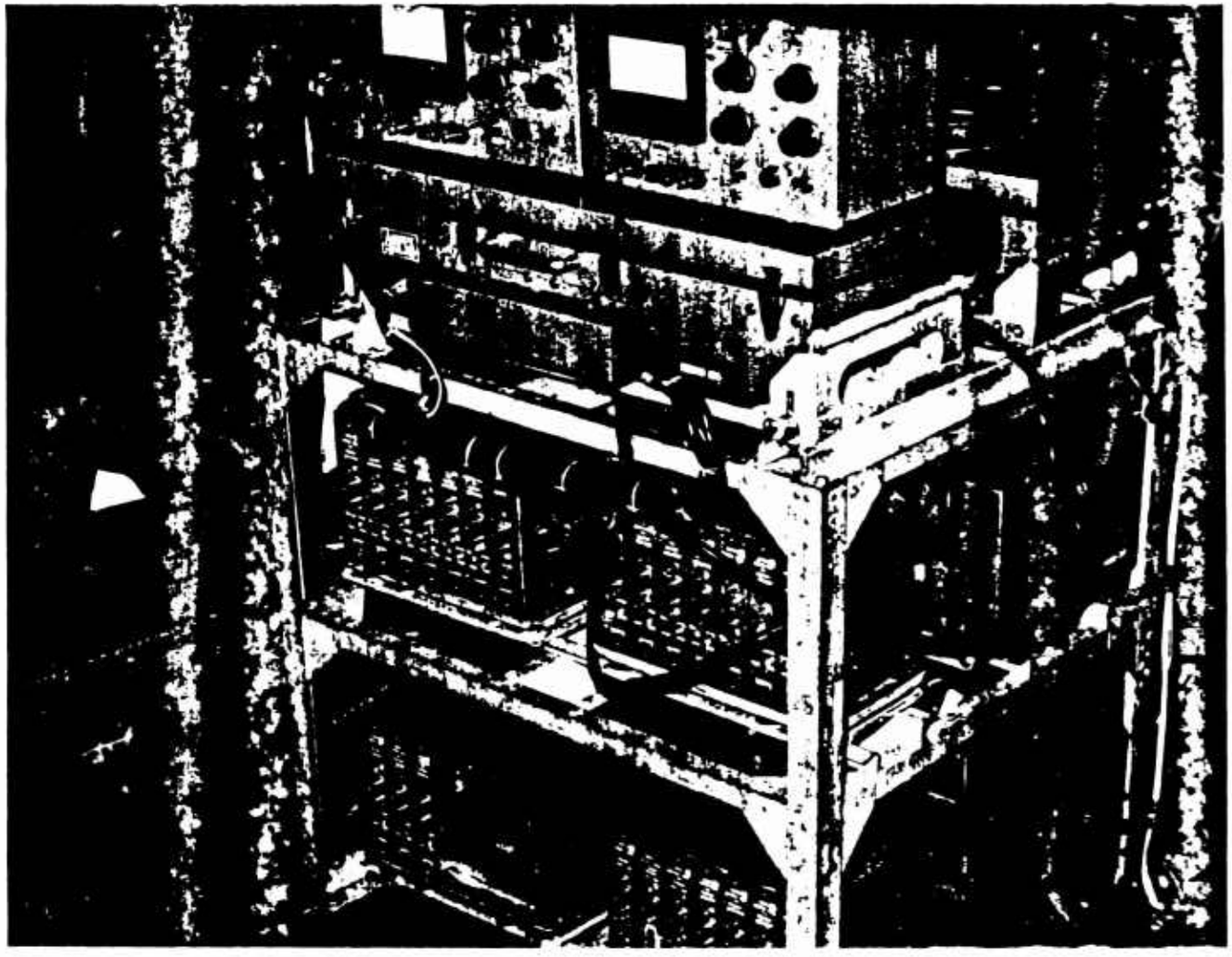

Figure 2.14 Ampex 800 magnetic tape recorders installed in aircraft.

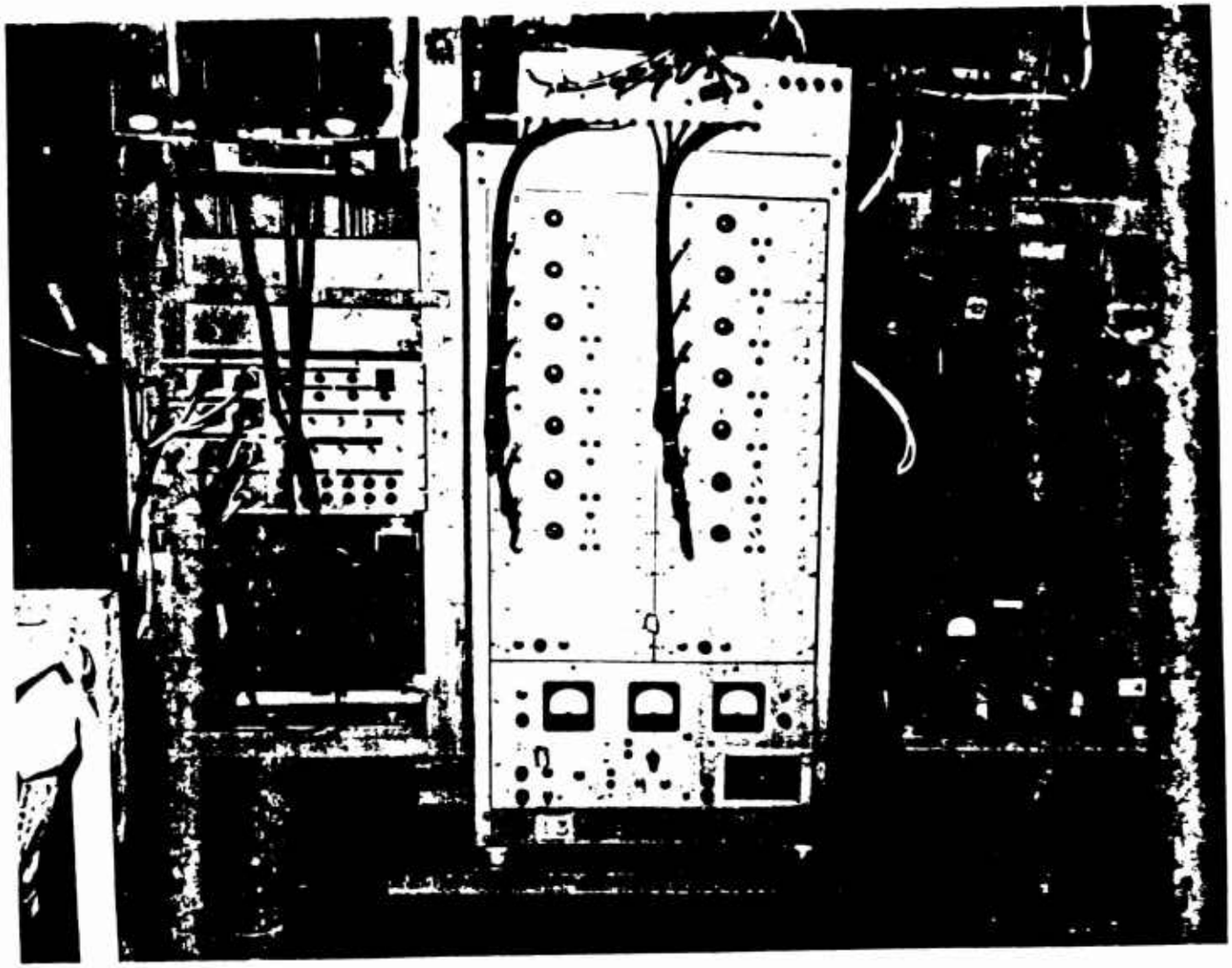

Figure 2.15 Amplifier console with sequence and calibrate cabinet installed in aircraft.

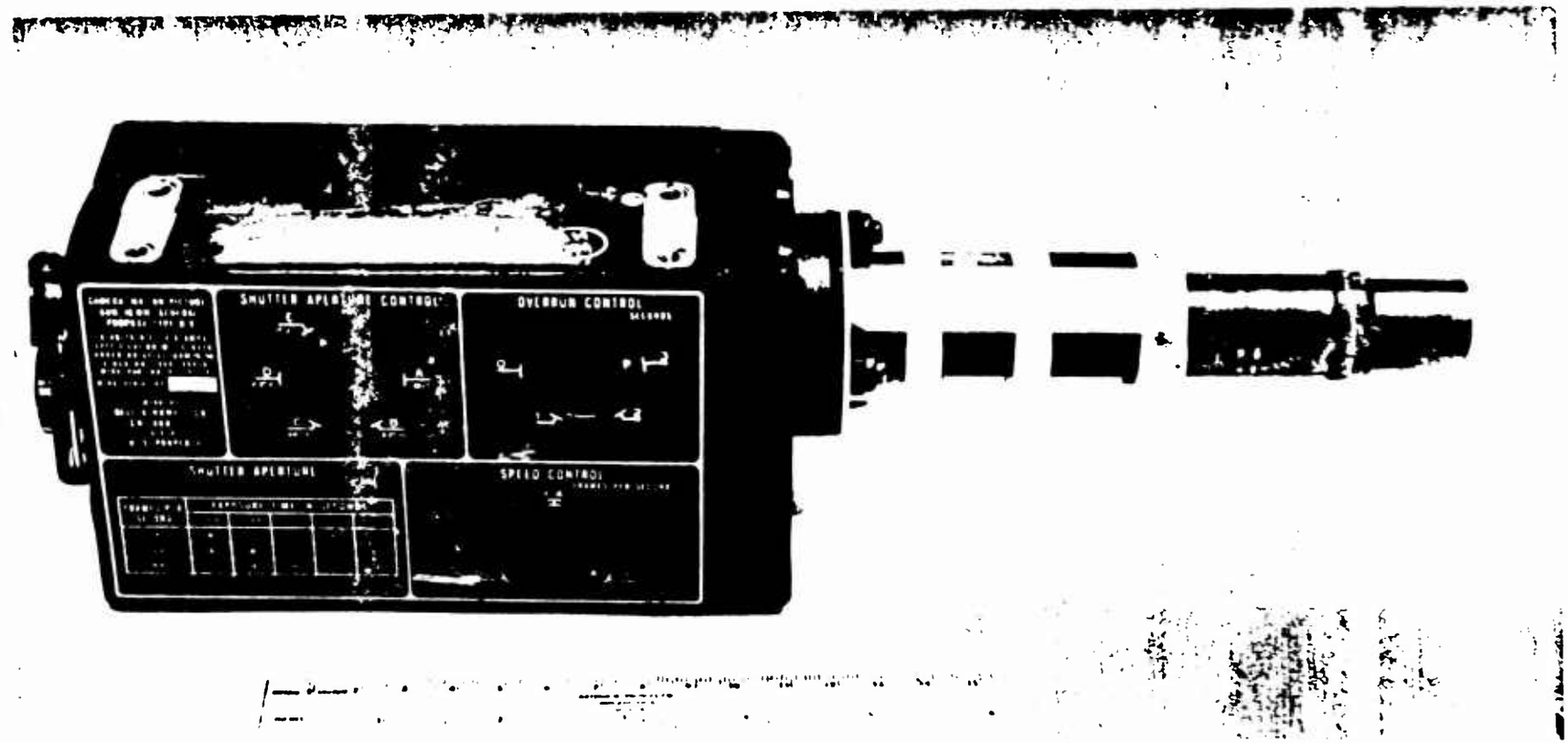

Figure 2.16 N-9 GSAP camera with spectroscopic nosepiece.

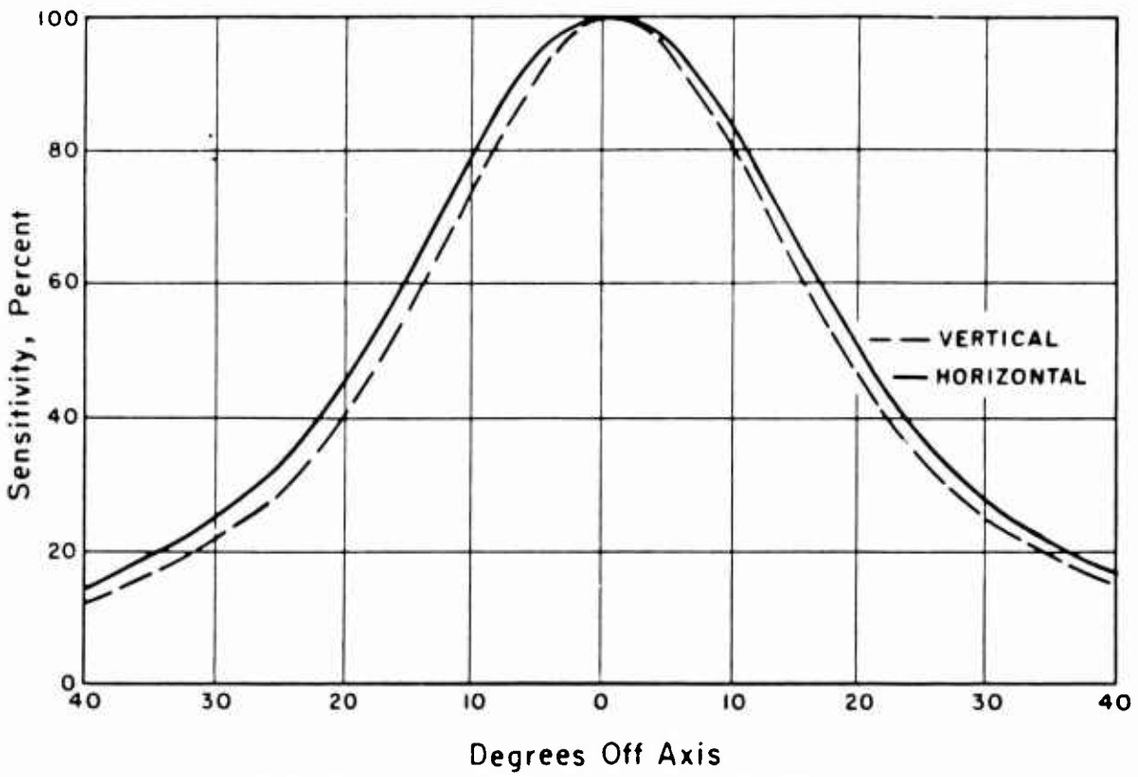

Figure 2.17 Field of view of NUV dispersion unit with diffuse window.

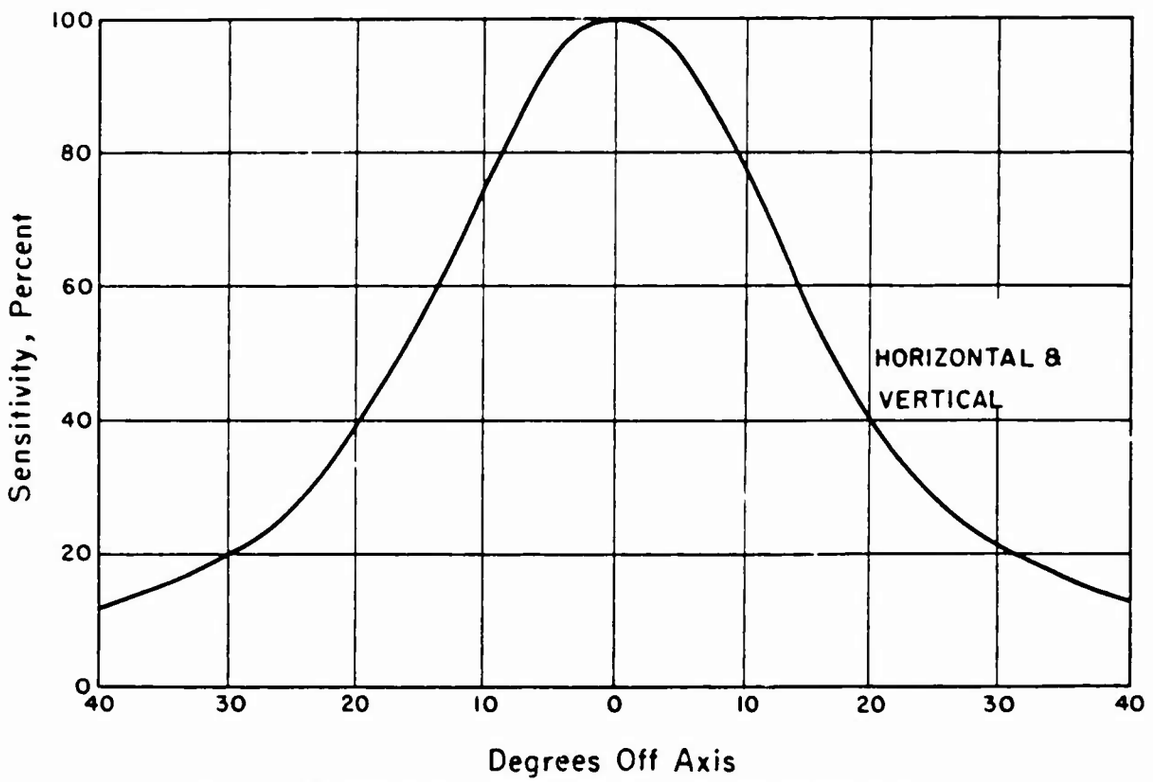

Figure 2.18 Field of view of VIS dispersion unit with diffuse window.

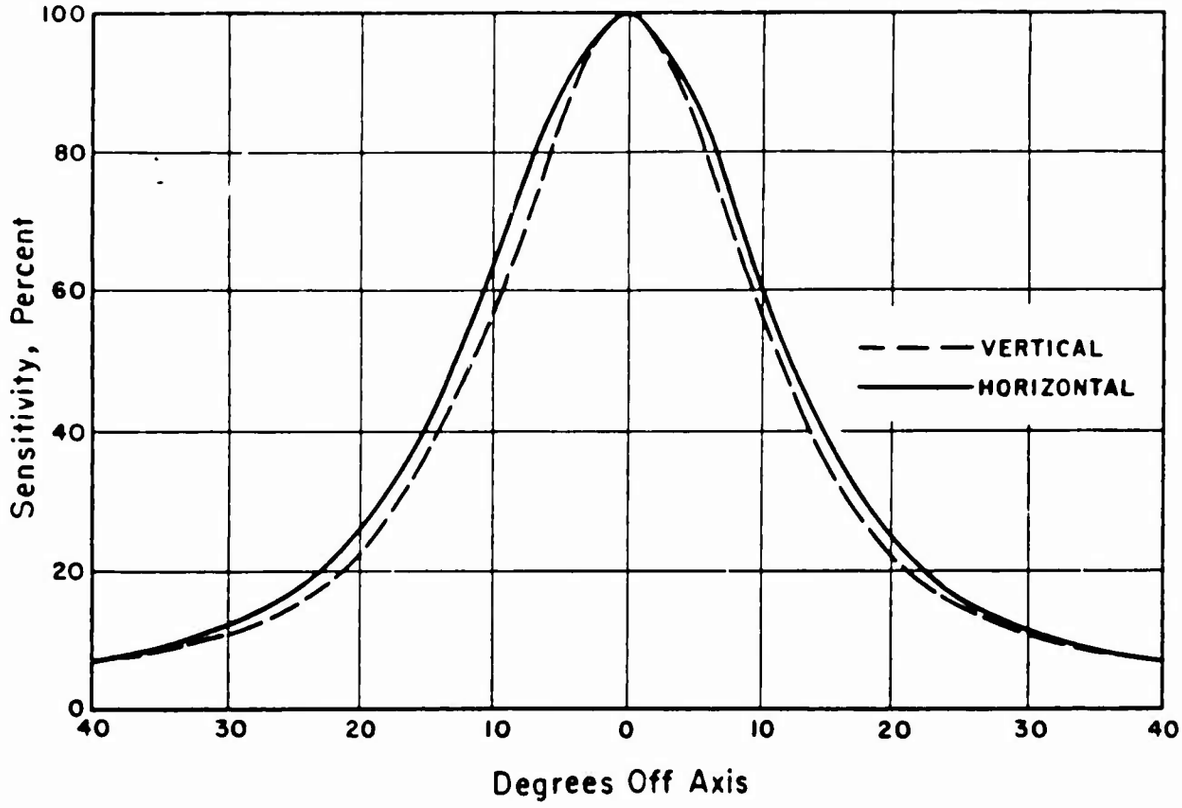

Figure 2.19 Field of view of IR dispersion unit with diffuse window.

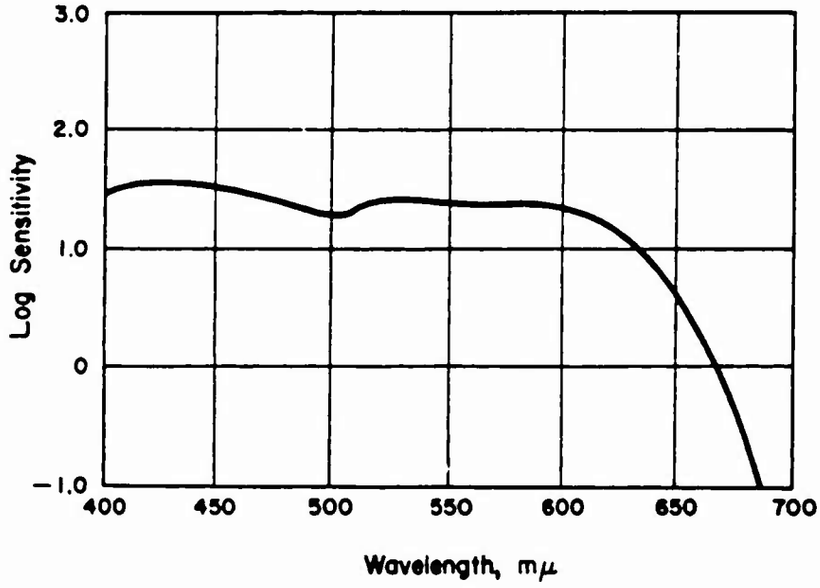

Figure 2.20 Sensitivity versus wavelength of Kodak 103-B film.

Figure 2.21 Ampex FR100A magnetic tape playback and Epsco analog-to-digital converter.

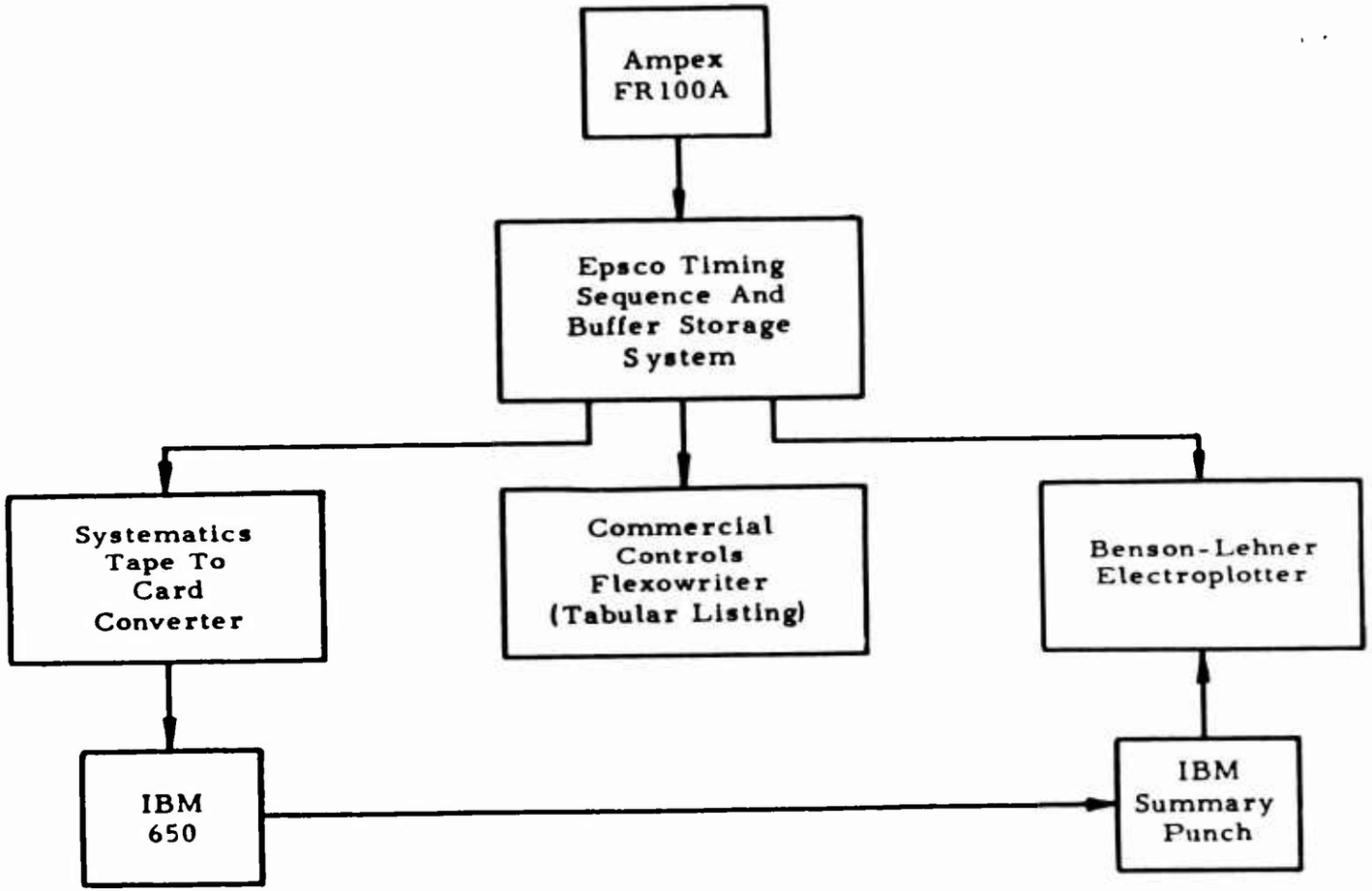

Figure 2.22 Block diagram of data reduction facility, thermal radiation laboratory, AFCRC.

Chapter 3

RESULTS

Thermal irradiance in each of the four spectral regions — FUV, NUV, VIS, and IR (Table 1.2) — was measured by dispersion units in the aircraft on Shots Yucca, Orange, and Teak. The thermal pulses were also recorded with the bolometers, and cinespectrographic information was obtained on all shots. The calorimeter was used only on Yucca and Teak and did not obtain data on either. For Yucca the instrument sensitivity was too low, and for Teak the calorimeter amplifier failed because of a power fluctuation that occurred just prior to detonation.

No measurements were obtained from the instrumented dragline canisters used on Shot Yucca. Approximately 2 minutes before zero time, a power surge disabled the shipboard command transmitter, which was required to initiate the canister recorder and delay playback systems. A continuously transmitting link was also provided in each canister as a backup for data recovery. This system functioned properly prior to zero time in the canisters at 1,050 and 1,500 feet from the device. The telemetry link was never closed with the third canister at 2,150 feet. However, immediately after detonation, there occurred a VHF blackout caused by ionization. After 4 seconds, telemetry was again received from the canister originally at 1,050 feet; however, the thermal pulse was over before this time. After zero time, the canister located at 1,500 feet was not heard from again. This particular canister used a modified dipole antenna, which is believed to have been destroyed by the detonation.

Curves of irradiance as a function of time in the various spectral ranges for all three bursts are presented in Figures 3.1 through 3.23. The ordinate values (w/cm^2) include the corrections for pointing error and window transmission as noted in Table 3.1; hence, they represent the actual irradiance at the aircraft. Pointing errors (degrees off optical axis) were determined from the documentary pictures shown in Figures 3.24 through 3.26. These corrections assumed that the fireball was a point source. An appreciable extended source would affect these values because of the decreased instrument sensitivity as the source deviates from the optical axis (Figures 2.17 through 2.19). Although the curves presented are not shown returning to zero in every case, the actual oscillograph traces were read out to zero irradiance for the purposes of obtaining the total energy received in each spectral range. Zero irradiance is defined here as signal/noise = 1 rather than in absolute terms.

The early portions of the pulses are also presented in expanded form (shorter time scale) to give detail of the more rapid variations at short times such as during the rise to peak values. Fluctuations of the order of 100μsec can be discerned in most of the expanded curves; however, faster variations are distorted because of the limited high-frequency response of the detection system.

Figures 3.27 through 3.29 present plots of the percentage of thermal energy delivered for wavelengths less than 1μ as a function of time for Yucca, Orange, and Teak, respectively. These plots show graphically the rate of delivery of the thermal energy. They do not include wavelengths greater than 1.0μ, because the bolometer amplifier produced a

nonlinear phase shift in frequencies below 100 cps and had a low frequency cutoff of about 5 cps, which combined to distort the more slowly varying portions of the pulse.

The bolometer measurements of peak irradiances are listed along with the data for each spectral region in Tables 3.2 through 3.4. Peak irradiance values, times to maxima (and minima on Yucca), and the total energy received (obtained by integration of the irradiance curves) are given for each spectral region. For the Orange and Teak bursts, irradiance values at selected later times are also listed.

The cinespectrographic results from Shots Yucca and Orange, which do not show regular structure, are not presented. This film data has been reduced to plots of energy incident on the film surface versus wavelength; however, the transmission of the nonepieces as a function of wavelength is still in the process of being determined.

The photographic results from Shot Teak, which yield line structure, are shown in Figures 3.30 through 3.34. The values of time indicated on the curves are the times as determined from time zero and are arrived at by the nominal values of frame speed characteristic of the cameras. The margin of error is due to the uncertainty in establishing time zero on the film record. Wavelengths observed on the teak records are listed in Table 3.5. The total accuracy of the reduction and detection system yields wavelength values accurate to ± 15 A.

The results presented in this chapter are those obtained at the aircraft. In Chapter 4 it is necessary to use various assumptions, such as atmospheric transmission and a point source approximation, to generalize the thermal information. Therefore, it is recommended that any independent work begin with the primary results presented in this chapter.

TABLE 3.1 CORRECTION FACTORS APPLIED TO RAW THERMAL DATA

Shot	Spectral Range	Pointing* Error	Window† Transmission
Yucca	FUV	0.12	0.80
	NUV	0.12	0.90
	VIS	0.12	0.75
	IR	0.12	0.62
	Bolometer	None	0.55
Orange	FUV	0.06	0.80
	NUV	0.06	0.90
	VIS	0.06	0.90
	IR	0.10	0.90
	Bolometer	None	0.90
Teak	FUV	0.02	0.80
	NUV	0.02	0.90
	VIS	0.02	0.90
	IR	0.04	0.90
	Bolometer	None	0.90

* These numbers represent the factor by which the sensitivity was reduced, because the burst was off the opitcal axis.

† These numbers are average values for the spectral region.

TABLE 3.2 THERMAL DATA AT AIRCRAFT, SHOT YUCCA

TABLE 3.3 THERMAL DATA AT AIRCRAFT, SHOT ORANGE

TABLE 3.4 THERMAL DATA AT AIRCRAFT, SHOT TEAK

pages 46 through 56 deleted.

TABLE 3.5 WAVELENGTHS OBSERVED AT 7.5 ± 2.5 msec, SHOT TEAK

Wavelength	Relative Intensity	Wavelength	Relative Intensity	Wavelength	Relative Intensity
A		A		A	
4,217	6.12	4,363	8.41	5,062	7.69
4,235	5.15	4,661	10.00	5,095	4.89
4,262	4.88	4,694	8.91	5,143	7.23
4,300	5.27	4,711	9.82	5,201	7.21
4,320	5.92	4,722	10.00	5,307	5.98
4,357	5.62	4,739	8.61	5,340	7.78
4,376	6.55	4,772	7.57	5,462	5.50
4,418	5.33	4,811	6.40	5,549	6.12
4,438	5.48	4,835	7.57	5,607	5.40
4,459	8.22	3,866	6.43	5,666	5.98
4,478	8.71	4,896	5.40	5,744	5.30
4,516	9.77	4,945	5.72	5,820	5.15
4,560	9.51	4,996	5.52	5,996	5.37
4,577	4.89	5,023	6.47	6,083	4.82
4,617	8.19	—	—	—	—

Figure 3.23 Expanded first peak in the bolometer, 2,000 to 36,000 A (3.6 μ), Shot Teak.

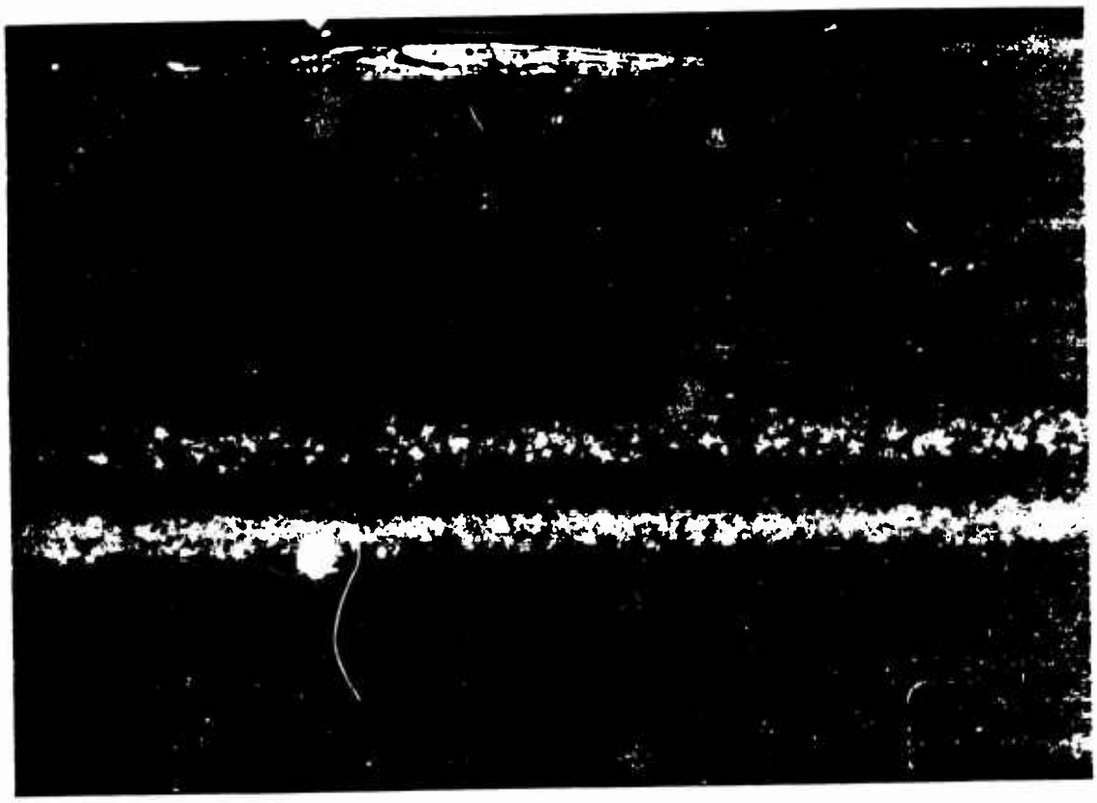

Figure 3.24 Photograph of Shot Yucca utilized to provide pointing error.

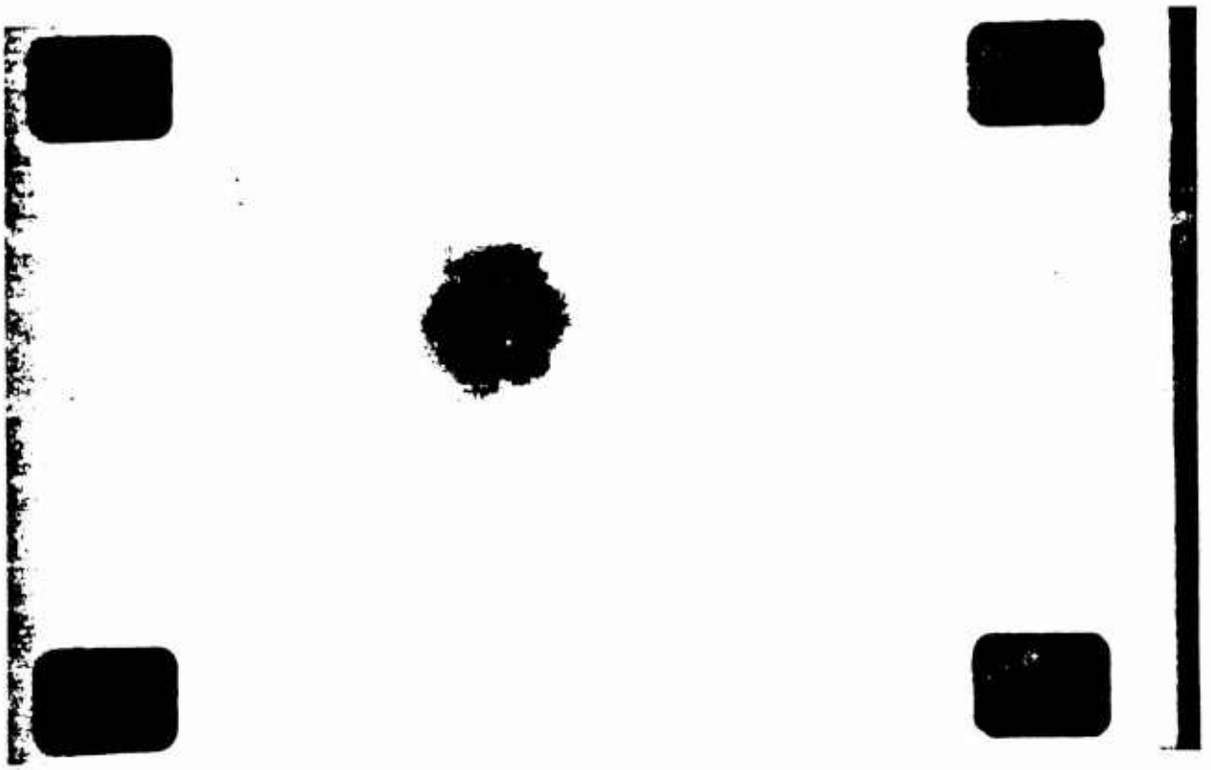

Figure 3.25 Photograph of Shot Orange utilized to provide pointing error.

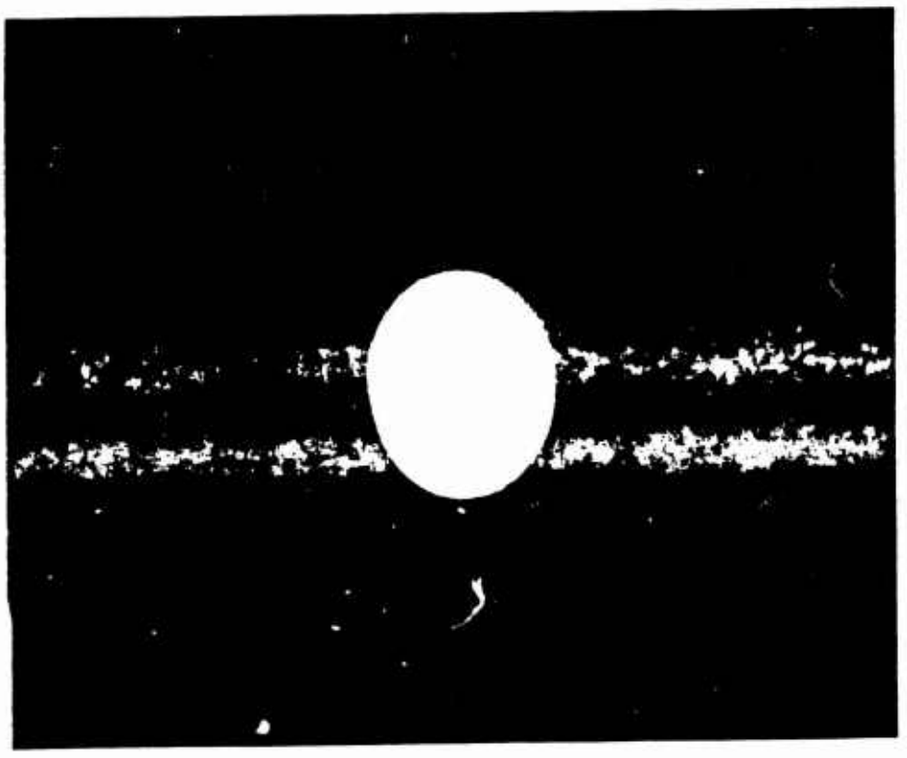

Figure 3.26 Photograph of Shot Teak utilized to provide pointing error.

pages 59 through 64
deleted.

Chapter 4

DISCUSSION OF RESULTS

4.1 DATA RELIABILITY

The procedures used in detecting, recording, and reducing the thermal data have been described in Chapter 2. The capabilities of the system are given in References 19 and 20. The high-frequency response of the overall system, which was limited primarily by the shunt capacities of transmission lines and frequency response of the preamplifiers, was approximately 7 kc. This would tend to obscure fluctuations shorter than 50μsec. The primary factors that caused limitations on the absolute irradiance values obtained by the dispersion units were the lack of sharp cutoffs of the spectral pass-band and the deviation from flatness of the response versus wavelength. These calibrations as well as the sensitivities of the various units that obtained data are given in Tables 2.1 through 2.3. In general, a number of dispersion units obtained data on each shot and thus increased the reliability of these measurements.

The phase shift of the bolometer amplifiers has not, as yet, been completely determined; however, it is known that the system experiences a nonlinear phase shift for frequencies below 100 cps, thus the late time information (t > 5 msec) from the bolometer is not presented in this report. Only one bolometer measured the signal from each burst, which did not allow the same degree of confidence as the dispersion unit data. Only preliminary postshot laboratory calibrations were obtained for the bolometers before they failed; however, these values were in rough agreement with the field calibrations using the sun as a standard source. Therefore, the bolometer data will be an upper bound, since sensitivities were primarily established by using a zenith sun and by assuming the maximum solar irradiance of 100 mw/cm^2 incident at sea level. A precise error figure has not been established for these measurements; however, it is felt that the upper bound bolometer data could be reduced by no more than 25 percent by possible calibration error.

To generalize the results obtained, it was necessary to estimate the atmospheric transmission and reduce the data to the source. Although atmospheric attenuation was not measured, some confidence in computations was possible, since the slant paths were always above an altitude of 30,000 feet, and, consequently, above a considerable portion of the turbulent atmosphere and water vapor. The detailed atmospheric transmission calculations are presented in Appendix A, and the resulting values used for each wavelength region as well as the respective slant ranges are given in Table 4.1.

4.2 EXPERIMENTAL-THEORETICAL COMPARISON

The data was reduced to an assumed point source, which introduced only a small error if the measurement distances were large compared with the source diameter. This was true if the source was not much larger than the visible fireball. The radiated power in each spectral region was thus obtained, and the thermal energy was derived by integration of the power-time curves.

The thermal measurements obtained by the FUV units were not utilized in this analysis. The relatively small irradiances measured in this region meant that scattered radiation of longer wavelengths within the instrument could have had a considerable effect, and the strong dependence of the atmospheric transmission in this wavelength region upon the unknown amount and distribution of ozone prevented meaningful calculations. Therefore, these measurements were not reduced to the burst point.

Spectrally resolved data showed no radiation was at the aircraft between 2,500 and 3,000 A (Reference 21). This was expected because of ozone absorption. For this reason the true short-wavelength cutoffs of the radiation received by the NUV units (designed for 2,500 to 4,000 A) has been taken at 3,000 A.

Figure 4.1 presents curves of black body radiation for various temperatures in the selected wavelength regions normalized to the radiation of wavelengths 0.3μ to 1μ, the region designated as "TOT." This graph can then be utilized to compare the reduced experimental results with black body radiation at various temperatures (Appendix B).

4.2.1 Shot Yucca. A summary of the results for Shot Yucca is presented in Table 4.2. Spectral power and times to the first and second maxima and to minimum are presented. As shown in the irradiance curves (Chapter 3), Yucca exhibited the characteristic thermal minimum and second maximum of lower altitude nuclear bursts. However, the usual scaling (Reference 22) no longer holds; for instance, use of where t_{min} is in milliseconds and W is the weapon yield in kilotons, gives for the predicted time to minimum. Similarly, for the time to second maximum. When compared to the experimental values of it is obvious that the thermal energy was delivered much faster than for sea level bursts. However, the extrapolated value of for the ratio of total thermal yield to weapon yield (shown in brackets in Table 4.2) is comparable with low-altitude nuclear detonations. As can be seen, is the figure obtained by integration of the irradiance curves (0.3μ to 1μ), and was calculated by assuming that the spectral distribution at late times was the same as at the first maximum. This is perhaps a lower bound, since the distribution at second maximum (compare Tables 4.3 and 4.4) indicates a larger percentage in the near infrared, as expected from a cooler radiator.

Tables 4.3 and 4.4 list some of the experimental results and various theoretical calculations. Peak powers in the various spectral bands are compared, and the data is converted into ratio form using 0.3μ to 1μ as the norm to aid in the comparison. It is apparent from Table 4.3 that the theoretical calculations of the first peak radiation rate (References 4 and 9) are within an order of magnitude of the experimental values. This fact plus comparison of the experimental ratio column ($\Delta\mu$/TOT) with the various predictions implies that Yucca did indeed radiate like a black body at early times.

Table 4.4 presents a similar layout of experimental and theoretical results for the second maximum; however, the late time pulse was not predicted by the models in References 4 and 9. Some preshot estimates (Reference 5) that used black body assumptions also for the second maximum are seen to agree within a factor of 2. Again, the ratio columns indicate that Yucca was still radiating much like a cooler black body even at such late times.

Figure 4.2 presents a theoretical curve of thermal radiation loss (Reference 9) in kilotons compared with the experimental curve (Figure 3.27). Agreement cannot be expected in comparison of absolute values of the thermal radiation at a given time, since the theoretical values were calculated for all wavelengths greater than the 0.186μ oxygen cutoff while the experimental measurements were restricted to a finite passband (0.3μ to 1μ). However, it should be noted that the slopes (rate of radiation) of the experimental and theoretical curve are in excellent agreement to times past the first maximum. The

theoretical treatment did not pretend to predict the radiation output past breakaway. Six percent of the thermal energy had been lost before breakaway versus a theoretical prediction of 10 percent.

4.2.2 Shot Orange. It is apparent from the irradiance curves of Chapter 3 (Figures 3.10 through 3.12) that the pulse shape for Shot Orange was considerably different from sea level megaton detonations. There was only a vestigial minimu n which occurred most markedly in the region of 0.5μ to 1μ at about 10 msec. Theoretical calculations (Reference 10) indicate that the explanation for this waveform was at least qualitatively similar to sea level bursts. In times like 5 to 10 msec, the hydrodynamic shock formed, and its radius became larger than that of the isothermal sphere. At these temperatures and densities, the shock was opaque and cooler than the isothermal sphere, so the rate of radiation dropped. As the shock cooled further, the Rosseland mean free path became long, the shock became transparent, and radiation was again received from the isothermal sphere. The expanding isothermal sphere maintained the radiation rate (note the plateau) until it also became transparent at about 200 msec and was no longer a good radiator. Figure 3.28 showed 86 percent of the thermal energy (0.3μ to 1μ) was radiated away by 200 msec.

Table 4.5 presents the generalized data (reduced to a point source) for Shot Orange. Perhaps the most unexpected result was the apparent shift in the spectral distribution toward the infrared. Column 2, for instance, shows that, at first maximum, more power was radiated at wavelengths greater than 1μ than in the region 0.3μ to 1μ. Although integration of the power-time curves gives the thermal energy radiated in the interval 0.3μ to 1μ, an extrapolation must be used to obtain the total thermal energy in the wavelength region 0.3μ to 3.6μ, since the bolometer did not obtain late time data. Because the field of view of the bolometer was greater than that of the dispersion units, a large source would be expected to produce a larger reading by the bolometer than by the dispersion units. It has been assumed that the angle subtended by the apparent source was small compared to the fields of view of the bolometer and dispersion units for this discussion.

The extrapolated integral bolometer figure of and the subsequent energy partition ratio of for thermal yield to weapon yield were obtained by assuming that the ratio $P_{max(BOLO)}/P_{max(TOT)}$ remained constant past 200 msec. That this assumption is qualitatively correct may be inferred by observing Table 4.6 where the irradiance data is again normalized, as for Shot Yucca, to the region 0.3μ to 1μ. As the fireball cools, Row 3 indicates that proportionately more and more of the radiation is in the near infrared region 0.5μ to 1μ. By implication then, it might be expected that the later P_{BOLO}/P_{TOT} ratio would be larger than, or at least of the same order as, the first maximum. It is to be noted that of the weapon yield appearing as thermal energy is a reasonable percentage for lower altitude and sea level bursts. Table 4.6 presents the power radiated by the source at various times and again compares with theoretical predictions at first maximum (Reference 4). Although the predictions are within an order of magnitude for all wavelength bands other than the 0.3μ to 0.4μ, the trend of the relative magnitudes as predicted by this black body model is just the reverse of the experimental values, as can be seen upon comparison of Columns 3 and 7.

Since the early fireball was expected to radiate like a black body, the yield was known, and the altitude was measured, and since the fireball size was determined photographically, an interesting upper bound theoretical-experimental comparison can be made. For air at a given density, the energy stored per unit volume in the form of kinetic energy, ionization energy, and energy of the radiation field is a function of the temperature of the medium. Hence, within a given volume if the total energy stored is known (for example, the yield of the nuclear device), within the visible fireball, then a temperature is defined.

Table 4.7 presents, for Shot Orange, the derived temperatures for various radii of the sphere within which the total yield is assumed to be contained (Reference 23). The exact size of the source contributing to the thermal measurements is taken to be unknown although the visible fireball radius was measured (Reference 24). Later time scanner measurements indicated a considerably larger infrared fireball (Reference 25). For of energy stored at this density and for the assumed radii, the energy in the radiation field never becomes comparable with the material energy stored. The power radiated in the wavelength intervals corresponding to the dispersion unit cutoffs is calculated for a black body source at the derived temperatures and assumed radii (Appendix B). The interval 0.186μ to 0.3μ is included, since this radiation escapes from the fireball. The bolometer region 1μ to 3.6μ is also tabulated. The calculated values in the table are upper bounds for the radiation emitted from sources with the given radii. The calculations for the fireball that was observed photographically (R = 0.9 km) are of particular interest.

At the bottom of Table 4.7, the measured powers are tabulated. The power between 1μ and 3.6μ is obtained by subtracting the sum of the dispersion unit values from the bolometer reading. This procedure is correct if the source was small within the field of view of both instruments.

If values calculated for the observed radius are considered, the power radiated in the region 0.3μ to 1μ is overestimated by factors between 7 and 70, whereas in the region 1μ to 3.6μ it is underestimated by about a factor of 2. It is obvious, and borne out by the calculations for other radii, that since the trend in the observed data is the opposite of that for a black body no change in the radius of the radiating sphere will produce an agreement.

Considering only the interval 0.3μ to 1μ, the observed data (Reference 26) could be explained by either a fireball with a low emissivity over this region, which is counter to prediction, or a black body radiating through a filter. However, the radiation received beyond 1μ requires the presence of a fluorescent medium between the source and the detector that will convert part of the more energetic radiation into infrared. It should again be noted at this point, however, that the figure of for 1μ to 3.6μ is an upper bound that was obtained by subtraction. This means that this number contains the possible errors of all of the separate numbers.

4.2.3 Shot Teak. Figures 3.17 through 3.19, the irradiance-time graph , show that Teak had no trace of the characteristic minimum and second maximum of low-altitude nuclear bursts. This indicates that, because of the late time of formation of hydrodynamic shock, it no longer had a large effect upon the thermal radiation pulse. However, Figure 3.29 shows that about of the thermal energy (0.3μ to 1μ) was radiated away by , just as for Orange.

The spectral data presented in Chapter 3 showed that radiation from the Teak fireball had strong emission line structure, but no quantitative statement can be made as to the magnitude of the underlying continuum. From tables of emissivity of hot air (Reference 27), it was expected that the fireball at this density would be partially transparent in the visible and ultraviolet; consequently, line structure might be expected. Theoretical calculations (References 11 and 12), which did not take line emission and absorption (bound-bound) into account, predicted the thermal radiation peak would occur later than the observed 0.5 msec and also underestimated the observed peak power. Figure 4.3 gives a comparison of experimental data with an early theoretical prediction (Reference 11). This graph illustrates how valuable this theoretical prediction proved to be for the preshot estimates of the instrumentation recording levels required.

Table 4.8 presents the thermal data obtained on Shot Teak reduced to an assumed point source. Again, as for Shot Orange, the spectral distribution of the radiation showed a

marked shift to the infrared. In fact, Teak exhibited even a larger ratio of the total thermal power at wavelengths greater than 1μ than did Orange. Again the total energy from 0.3μ to 3.6μ could only be estimated by comparing with the integrated value from 0.3μ to 1.0μ and assuming that $P_{max(BOLO)}/P_{max(TOT)}$ remained constant. Such an extrapolation yields a thermal yield to device yield ratio of (in brackets in Table 4.8) a number which is very high.

Just as for Shot Orange, the photographically observed radius of Shot Teak and other assumed radii were used to derive the black body radiating temperature. This is shown in Table 4.9 along with the observed values extrapolated back to a point source. Again, no such simple artifice as varying the source radius can bring these values into agreement with the observed values. The power radiated over the region 0.3μ to 1μ deviates even more strongly from the black body estimates than was the case in Shot Orange. The radiation beyond 1μ, obtained experimentally (again by subtraction), exceeds by factors of 4 to 6 that expected from the various volumes of heated air, each radiating as a black body. Instrumentation errors are not nearly sufficient to explain the large observed infrared emission without some mechanism for degrading energy into the longer wavelengths.

There is a reasonable mechanism for creating such a fluorescing mantle of sensitized air for these high-altitude bursts. The X-rays heat the air in the near regions of the device to incandescence. This fireball will then, in general, be viewed through the surrounding cold medium; however, this medium should not be considered normal air. An appreciable fraction of the X-rays, gamma rays, and, at times greater than a few milliseconds when the device is sufficiently disassembled, the energetic electrons from beta decay of the fission products will deposit their energy (primarily through ionization) in the regions exterior to the visible fireball without appreciably heating the air.

The size and nature of this mantle is strongly dependent upon the altitude of the burst and the position in question. For example, for a shot such as Teak, the range of the beta rays is about 50 km at co-altitude but only about 15 km in the downward direction. Again, the formation time of various species varies strongly with altitude; at 80 km the attachment time to form 0^- is about 0.5 sec; at 50 km it is of the order of a millisecond.

Hence, the detailed composition of the surrounding air (that is, the fractional amount of N_2^+, 0^+, 0^-, 0_2^-, free electrons, and any compounds such as N0) cannot be obtained from equilibrium considerations, since the air is not in kinetic, let alone thermodynamic, equilibrium. This modified air must be examined in detail to determine the absorption and emission that will take place over the thermal spectrum.

TABLE 4.1 SLANT RANGES AND ATMOSPHERIC TRANSMISSIONS

Shot	Slant Range	FUV	Atmospheric Transmission			Bolometer†
			NUV*	VIS	IR	
	km					
Yucca	24.5	—	0.65	0.32	0.98	0.90
Orange	138	—	0.42	0.75	0.92	0.90
Teak	137	—	0.63	0.86	0.95	0.90

* For 0.3μ to 0.4μ. It was experimentally determined that no radiation of 0.25μ to 0.3μ reached the aircraft.

† 0.2μ to 3.6μ.

70 pages through 75 deleted.

Chapter 5

CONCLUSIONS AND RECOMMENDATIONS

5.1 CONCLUSIONS

The results as discussed in Chapter 4, where the experimental data on Orange and Teak showed more infrared emission than could be radiated by a black body of dimensions comparable with those of the visible fireball, pose very important scientific questions

Careful consideration has been given to the validity of the experimental results. However, a detailed investigation has lead to the conclusion that these values are realistic. The same instruments and procedures were also used to obtain thermal data on 10 sea level, low-yield devices during Operation Hardtack, Phase II (Project 8.8). It is of interest to note that in all of the Phase II data (final version of Reference 20 to be published as WT-1675) the preliminary results are consistent with previous measurements on sea level detonations, and the amount of radiation in the infrared agrees with that expected from black body radiators. In general, the bolometer measurements on Phase II are only slightly greater than the sum of the dispersion unit values, as is to be expected, since the bolometers detect radiation over a larger wavelength range. Such experience with this newly developed instrumentation system gives confidence in the results.

A more detailed and exhaustive approach in describing thermal radiation from high-altitude nuclear bursts than the equilibrium-opacity theory, which works satisfactorily for low-altitude bursts, is obviously necessary to explain these experimental results. It is necessary to postulate some nonequilibrium mechanism that increases radiation levels in the infrared beyond the equilibrium black body theory. The possibility of various species, such as NO or O^-, emitting very strongly in the infrared is recognized, but the details of the formation and excitation of such species in the vicinity of a high-altitude nuclear burst are, as yet, poorly understood.

Another piece of experimental information that could shed light on the problem is the size of the infrared fireball. The infrared picture of Teak, obtained by a modified AN/AAS-4(XA-2) infrared mapping device (Reference 25), shows an inner core, presumably the visible fireball, surrounded by a much larger radiating infrared fireball.

One of the difficulties is the present lack of calculations on the absorption and emission properties of relatively cold air that has been strongly ionized. An obvious conclusion as a result of the data obtained is that simple scaling laws cannot describe the phenomena as the altitude of the burst increases, particularly past 100,000 feet.

5.2 RECOMMENDATIONS

The thermal measurements obtained on Shots Orange and Teak have raised very important questions concerning the general thermal military problem for high-altitude nuclear bursts. The nature of the measurements were too gross to allow a complete determination or even a rough description of the thermal phenomena. From the comparison of experimental results with the considerable theoretical efforts, it is apparent that much more data

and theoretical work are required. It would be invaluable to obtain absolute spectral irradiance with better spectral resolution (particularly in the infrared) from various positions proximate to a high-altitude burst such as Teak. Simultaneous measurements taken from above, at co-altitude, and from below would present the necessary comprehensive picture. Close-in measurements obtained at various ranges are also very important pieces of missing information.

It is recommended that theoretical and laboratory work be pursued on the properties of irradiated air, to check the possibility that air at low densities, sensitized by ultraviolet, X, γ, and β rays, could produce such a hypothesized fluorescent mantle.

Another almost totally unexpected aspect of these first high-altitude detonations was the spectacular, long-lasting, optical displays. Visible radiation was observable for at least 30 minutes after Shots Orange and Teak. Unfortunately, other than a few "curiosity" photographs, no measurements were obtained on these low-intensity, spatially extended effects, which may have important consequences for optical seeking and tracking systems, particularly in the infrared. It is imperative to pursue the possibilities of infrared blackout by high-altitude nuclear bursts, especially since the orbital early warning and boost kill AICBM systems are based upon the use of infrared sensors.

It is recommended that a strong theoretical, laboratory, and field program be pursued on these thermal problems. Simulation techniques should be investigated and utilized during moratorium periods to isolate and aid in understanding, one by one, the geophysical parameters involved. Full laboratory studies should be undertaken to obtain good basic numbers such as cross sections and transition probabilities, which are so important for theoretical investigations. The theory of high-altitude bursts must be reexamined carefully and expanded, taking into consideration the experimental results and experience gained during Operation Hardtack.

A great deal can be accomplished by such a sound approach, but nature being as it is, careful measurements of other high-altitude nuclear detonations must be obtained.

Appendix A

ATMOSPHERIC TRANSMISSION

The transmission of thermal radiation through the stratosphere is chiefly attenuated by ozone, water vapor, oxygen, and carbon dioxide absorption, and atmospheric scattering. The transmissions calculated here are for an instrument platform at approximately 40,000 feet looking along specific slant paths at detonations at altitudes of 85,000, 141,000, and 250,000 feet.

The region of the electromagnetic spectrum under primary consideration is from 0.2μ to 1.0μ. Figure A.1 indicates why measurements at wavelengths less than 0.2μ are not feasible for this program (Reference 28). Even below 0.3μ strong ozone and oxygen absorption together with atmospheric scattering should effectively blank out most of the radiation. There is evidence, however, that between the strong oxygen absorption of the Schumann-Runge continuum and the Huggins-Hartley bands there exists a transmission window at the altitudes under consideration. Photon counters, one of which was sensitive in the band from 1,725 to 2,100 A, were flown in a V-2 rocket (Reference 29); the counting rate, in this band, rose sharply at 7 km, and the tube was too sensitive to provide useful data above 20 km. The altitude at which the atmosphere above transmits 1- and 10-percent incident radiation is shown in Figure A.2 (Reference 30); this also indicates the possibility of a high-altitude window. It is estimated in a feasibility study (Reference 31) that the transmission for a shot similar to Yucca is approximately 5 percent in this window region.

An approximate measure of atmospheric transmission can be obtained by assuming that the intensity of a parallel beam decreases by a factor e^{-KU} where K is the attenuation coefficient per unit length, and U is the optical path length that the radiation traverses in the particular medium under consideration. The total attenuation coefficient K is defined as $K = K_1 + K_2$, where K_1 is the coefficient due to absorption by atmospheric constituents and K_2 is the coefficient due to atmospheric scattering.

Atmospheric scattering consists of large- and small-particle scattering. The small-particle, or Rayleigh, scattering ($a/\lambda << 1$, where a is the diameter of the scattering sphere and λ is the wavelength of interest) is characterized by the scattering coefficient being proportional to the inverse fourth power of the wavelength. Haze and most clouds are below the altitude of interest; hence, the scattering is considered to be pure Rayleigh (Reference 32). The attenuation coefficients are taken from theoretical calculations as presented in Reference 1. Appropriate path lengths are obtained by multiplying the reduced equivalent thickness from Table 16-19 of Reference 1 by the secant of the zenith angle.

The water vapor content of the atmosphere above the aircraft was not measured at the time of the shots. A value of 0.01 cm of precipitable water above the tropopause (Reference 33) is used for computational purposes. The values for transmittance of radiation through water vapor are found in Table 16-3 (Reference 1).

The ozone absorption coefficients used are taken from Table 16-16 (Reference 1). The total ozone amount and distribution—quantities which vary daily—also were not measured at the time of the shots; therefore, the values used are from the theoretical models shown in Figures A.3 and A.4 (Reference 34). The total ozone amount in a vertical column above the aircraft was multiplied by the secant of the zenith angle to give the path length of the radiation through ozone.

Carbon dioxide has no absorption bands at wavelengths less than 1μ; hence, this constituent can be disregarded for the purposes of this report.

Figures A.5 through A.7 are graphs of the calculated percent atmospheric transmission versus wavelength for Shots Yucca, Orange, and Teak. The tabular values used to prepare these graphs plus a transmission breakdown by the individual constituents are presented as Tables A.1 through A.3.

The transmission graphs presented in Figures A.5 through A.7 can be considered only rough approximations for the following reasons: (1) The ozone amount and distribution could have been substantially different from the theoretical model. (2) The calculations are based on an undisturbed atmosphere while in reality this was not the case. (3) No attempt is made to compute the transmission in the window region (0.2μ) because the oxygen absorption coefficients are not well known in this wavelength region. (4) For shorter wavelengths (NUV, VIS), the calculated atmospheric transmission will tend to be small, because the Rayleigh scattering computation takes into account only scattering out of the beam whereas in reality multiple scattering caused scatter back into the beam. Such a calculation is also complicated by the fact that the sensitivity of the detectors falls off sharply with increasing angle from the optical axis (Figures 2.17 through 2.19).

For wavelengths greater than 1μ, atmospheric transmission is dependent upon the amount and distribution

of H_2O and CO_2. The absorption bands in this region are strong, thus necessitating a knowledge of the wavelength distribution of the radiation or use of a narrow band detector. A transmission of 90 percent is used for the bolometer on all three shots.

TABLE A.1 ATMOSPHERIC TRANSMISSION, SHOT YUCCA

Wavelengths	K_1U_1*	K_2U_2†	t_{H_2O}	T‡
μ				
0.30	2.24	0.396	0.98	0.07
0.31	0.587	0.346	—	0.36
0.32	0.185	0.302	—	0.60
0.33	0.0186	0.265	—	0.74
0.34	0.0130	0.233	—	0.77
0.35	0.00174	0.206	—	0.80
0.36	—	0.183	—	0.82
0.37	—	0.163	—	0.83
0.38	—	0.146	—	0.85
0.39	—	0.131	—	0.86
0.40	—	0.118	0.98	0.87
0.41	—	0.106	—	0.88
0.42	—	0.0965	—	0.89
0.43	—	0.0875	—	0.90
0.44	—	0.0795	—	0.90
0.45	—	0.0725	—	0.91
0.46	—	0.0663	—	0.92
0.47	—	0.0606	—	0.93
0.48	—	0.0556	—	0.93
0.49	—	0.0512	—	0.93
0.50	—	0.0470	0.99	0.94
0.55	0.0191	0.0320	—	0.94
0.60	0.0292	0.0222	—	0.94
0.65	0.0147	0.0162	—	0.96
0.70	0.00473	0.0119	—	0.97
0.80	—	0.00696	—	0.98
0.90	—	0.00435	0.96	0.96
1.00	—	0.00282	0.99	0.99

* K_1U_1 is the ozone absorption coefficient times the optical path length.

† K_2U_2 is the Rayleigh scattering coefficient times the optical path length.

‡ $T = e^{-KU} \times t$, where t is the water vapor transmission, and $e^{-KU} = e^{-(K_1U_1 + K_2U_2)}$.

TABLE A.2 ATMOSPHERIC TRANSMISSION, SHOT ORANGE

Wavelengths	K_1U_1*	K_2U_2†	t_{H_2O}	T‡
μ				
0.30	7.44	1.45	0.97	—
0.31	1.95	1.27	—	0.04
0.32	0.610	1.11	—	0.17
0.33	0.0617	0.975	—	0.34
0.34	0.0430	0.855	—	0.40
0.35	0.00576	0.757	—	0.45
0.36	—	0.674	—	0.50
0.37	—	0.600	—	0.53
0.38	—	0.537	—	0.57
0.39	—	0.481	—	0.60
0.40	—	0.434	0.97	0.63
0.41	—	0.392	—	0.66
0.42	—	0.354	—	0.68
0.43	—	0.322	—	0.70
0.44	—	0.292	—	0.73
0.45	—	0.266	—	0.75
0.46	—	0.244	—	0.77
0.47	0.00665	0.222	—	0.78
0.48	0.0125	0.204	—	0.79
0.49	0.0156	0.188	—	0.80
0.50	0.0305	0.173	0.98	0.80
0.55	0.0656	0.117	—	0.82
0.60	0.0970	0.0821	0.99	0.82
0.65	0.0493	0.0595	—	0.88
0.70	0.0164	0.0440	0.99	0.93
0.75	0.00782	0.0332	—	0.95
0.80	—	0.0256	0.98	0.96
0.90	—	0.0160	0.95	0.94
1.00	—	0.0104	0.99	0.98

* K_1U_1 is the ozone absorption coefficient times the optical path length.

† K_2U_2 is the Rayleigh scattering coefficient times the optical path length.

‡ $T = e^{-KU} \times t$, where t is the water vapor transmission, and $e^{-KU} = e^{-(K_1U_1 + K_2U_2)}$.

TABLE A.3 ATMOSPHERIC TRANSMISSION, SHOT TEAK

Wavelengths	K_1U_1*	K_2U_2†	t_{H_2O}	T‡
μ				
0.30	3.69	0.727	0.98	0.01
0.31	0.965	0.631	—	0.20
0.32	0.303	0.551	—	0.42
0.33	0.0307	0.485	—	0.59
0.34	0.0214	0.426	—	0.63
0.35	0.00286	0.376	—	0.67
0.36	0.000683	0.335	—	0.70
0.37	—	0.296	—	0.73
0.38	—	0.267	—	0.75
0.39	—	0.239	—	0.77
0.40	—	0.216	0.98	0.79
0.41	—	0.195	—	0.81
0.42	—	0.176	—	0.82
0.43	—	0.160	—	0.84
0.44	—	0.145	—	0.85
0.45	—	0.133	—	0.86
0.46	—	0.121	—	0.87
0.47	0.00330	0.111	—	0.88
0.48	0.00620	0.102	—	0.89
0.49	0.00776	0.0935	—	0.89
0.50	0.0151	0.0860	0.99	0.89
0.55	0.0326	0.585	—	0.90
0.60	0.0481	0.0408	—	0.91
0.65	0.0244	0.296	—	0.94
0.70	0.00815	0.0219	—	0.96
0.75	0.00388	0.0165	—	0.96
0.80	—	0.0127	0.99	0.97
0.90	—	0.00793	0.96	0.96
1.00	—	0.00518	0.99	0.99

* K_1U_1 is the ozone absorption coefficient times the optical path length.

† K_2U_2 is the Rayleigh scattering coefficient times the optical path length.

‡ $T = e^{-KU} \times t$, where t is the water vapor transmission, and $e^{-KU} = e^{-(K_1U_1 + K_2U_2)}$.

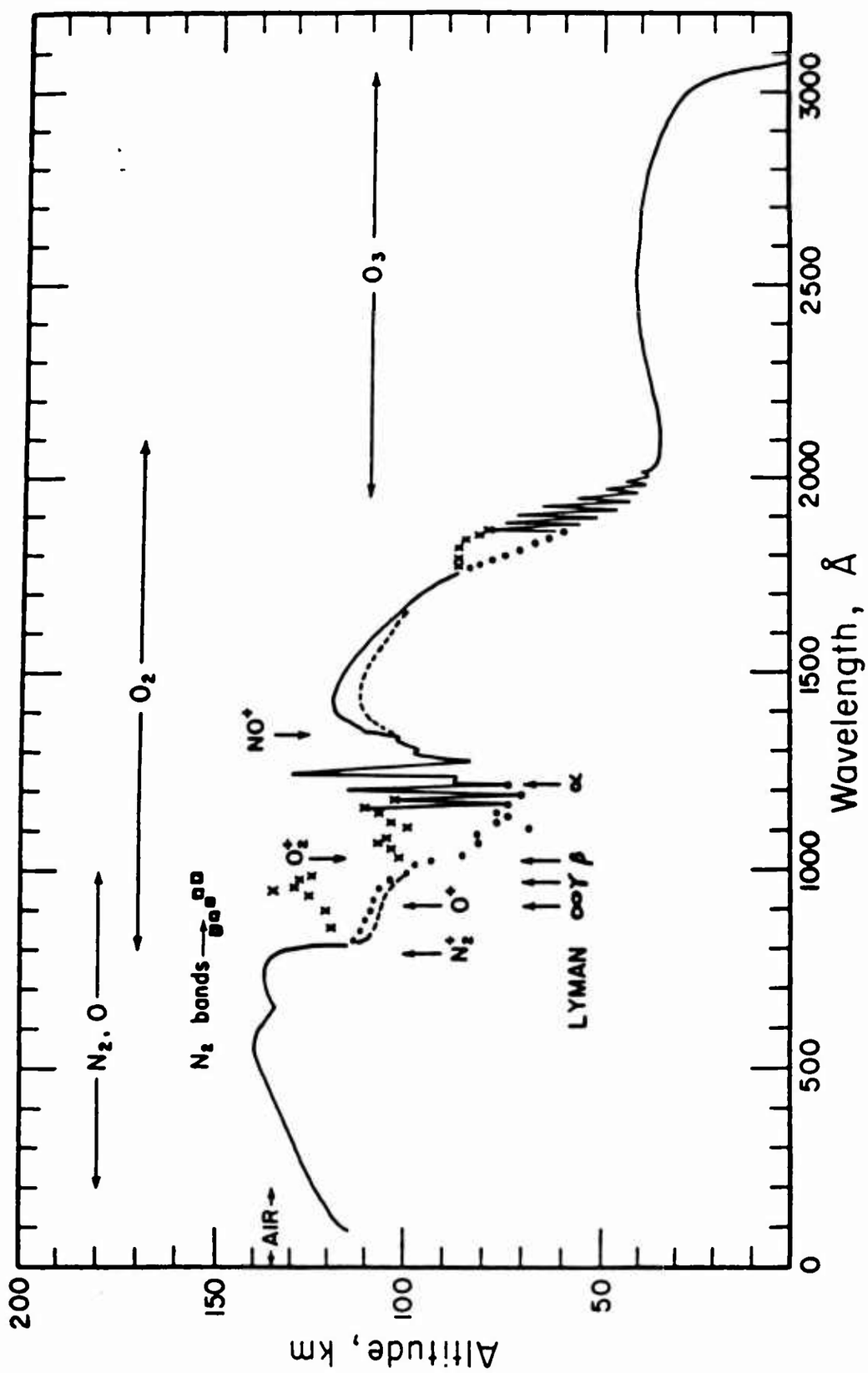

Figure A.1 Altitude at which intensity of solar radiation at vertical incidence is reduced by a factor e.

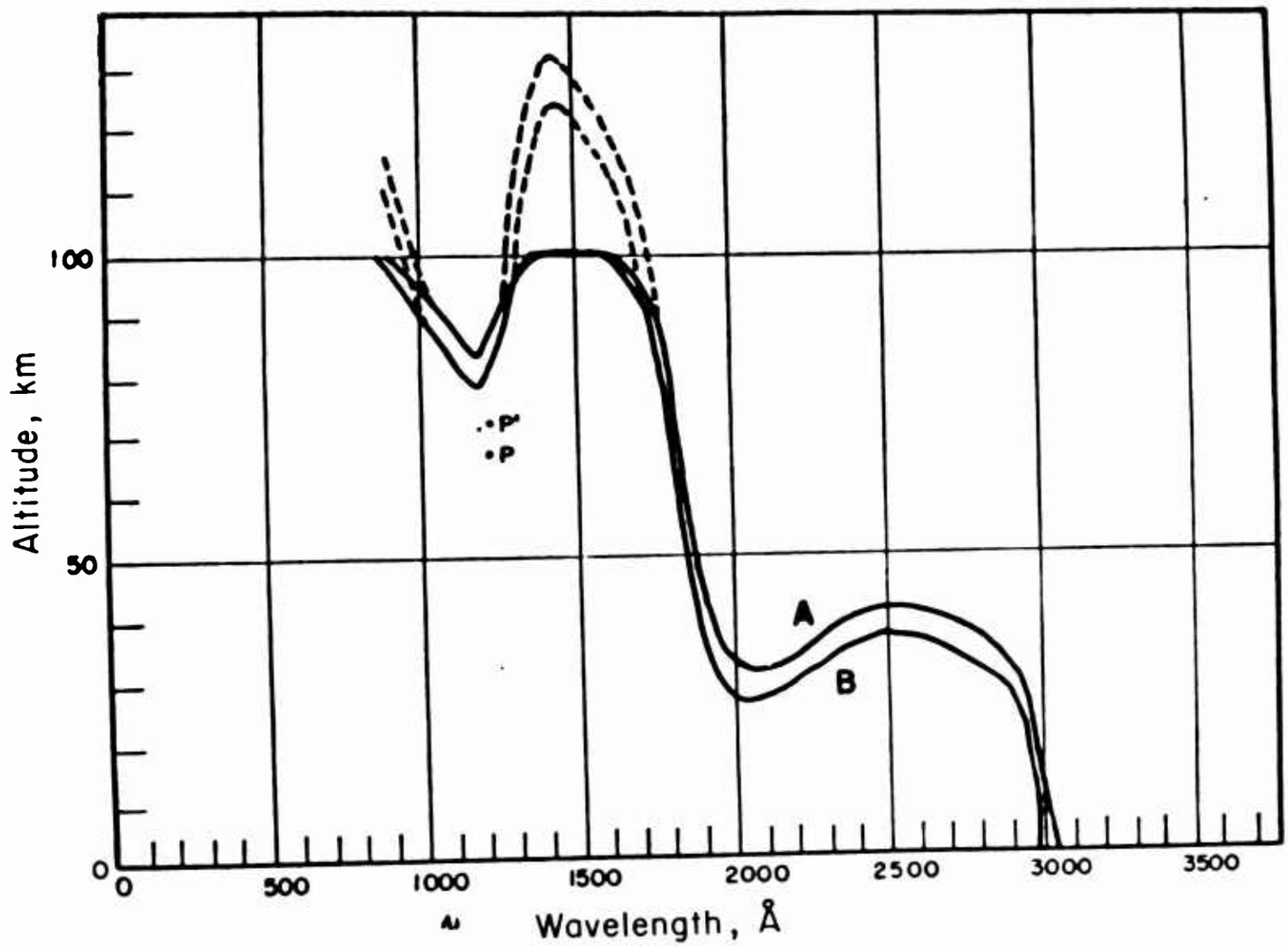

Figure A.2 Altitude at which atmosphere above transmits 1- and 10-percent incident radiation. Curve A is for 10 percent, and Curve B is for 1 percent.

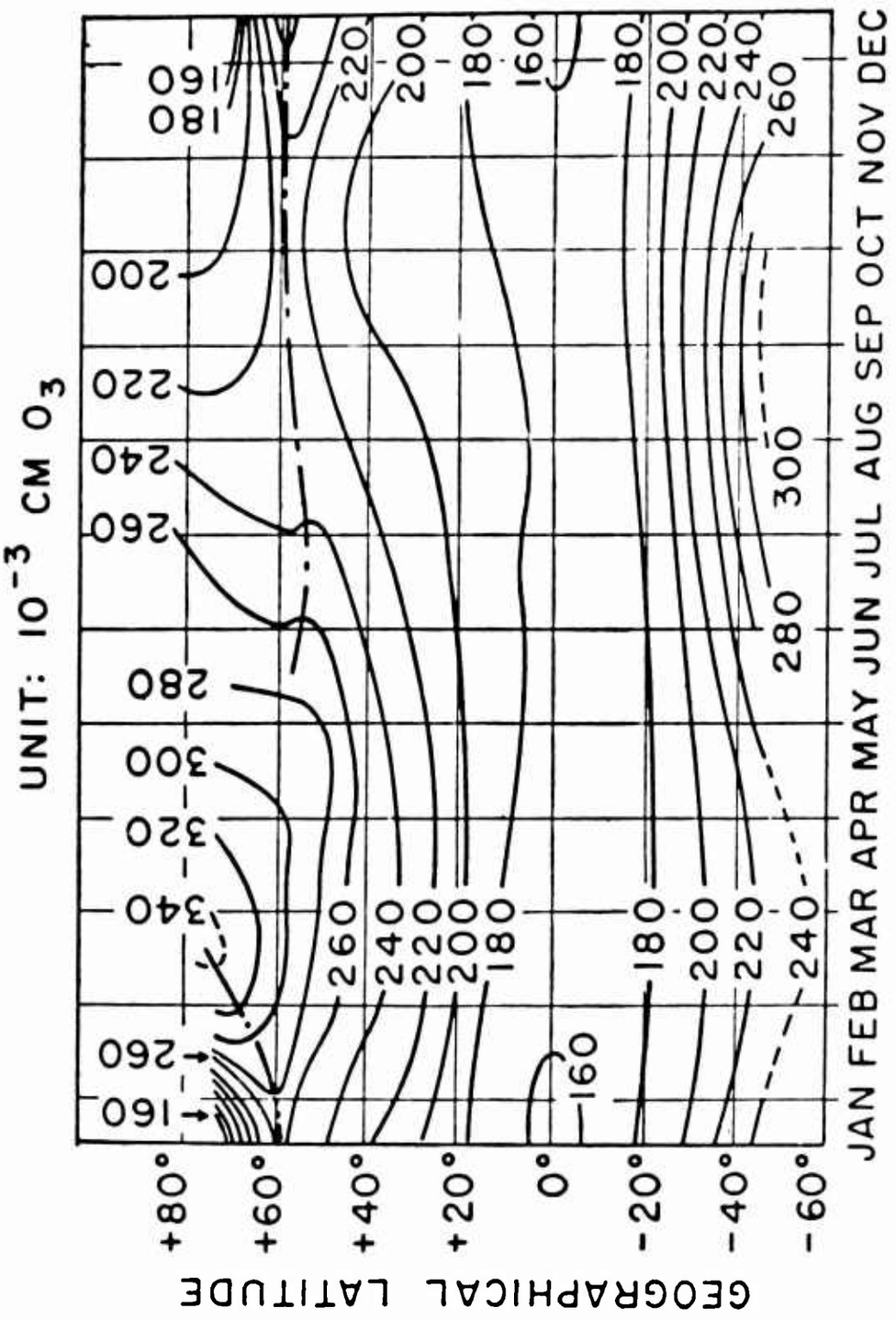

Figure A.3 Isopleths of the average ozone amount.

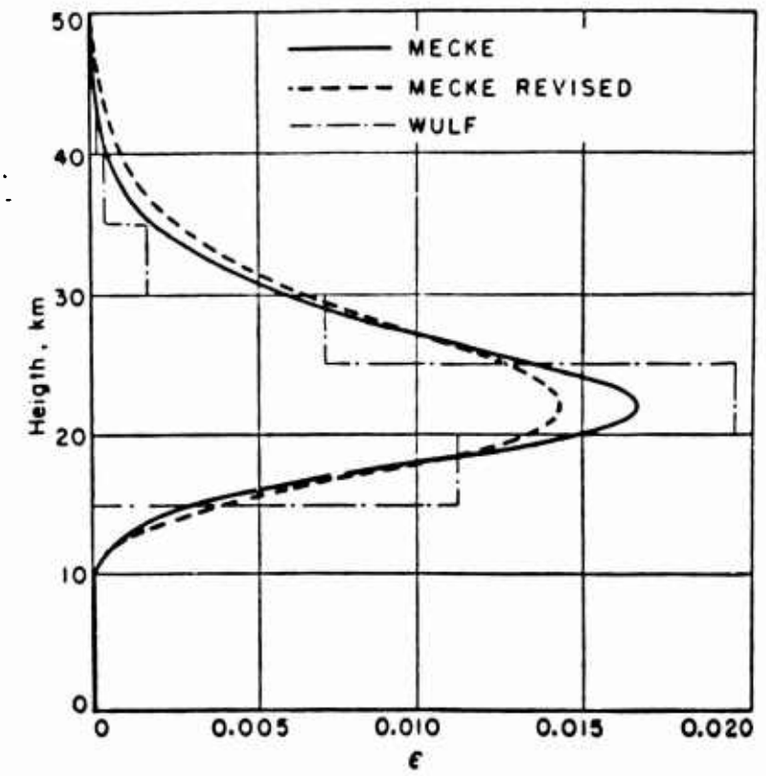

Figure A.4 Vertical ozone distribution.

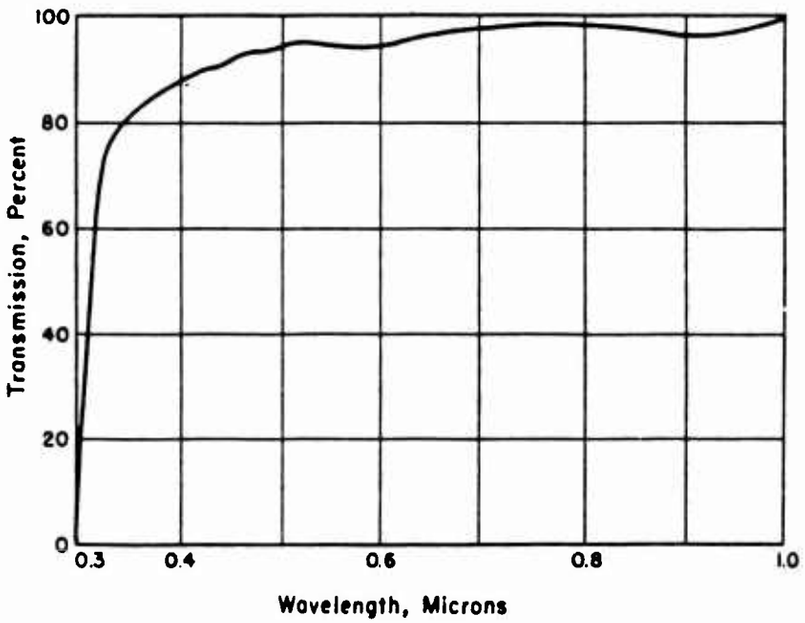

Figure A.5 Atmospheric transmission, Shot Yucca.

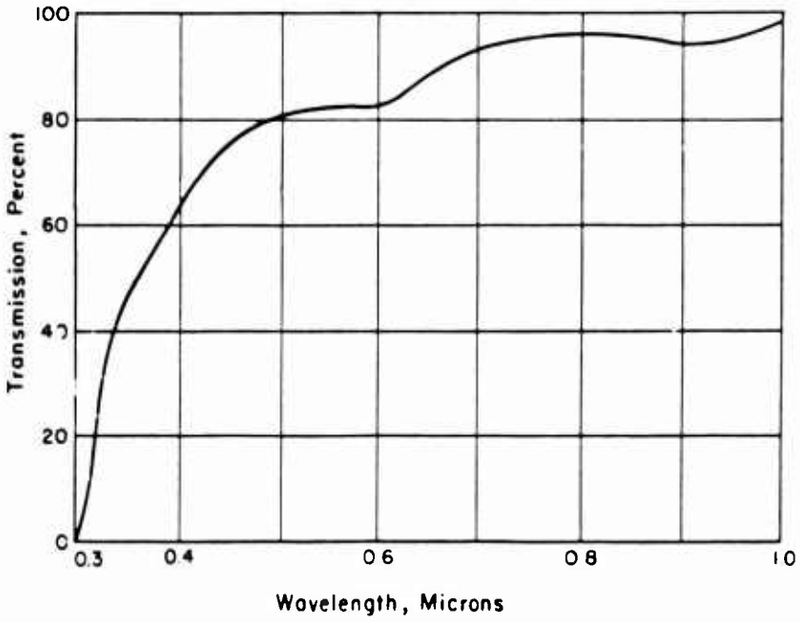

Figure A.6 Atmospheric transmission, Shot Orange.

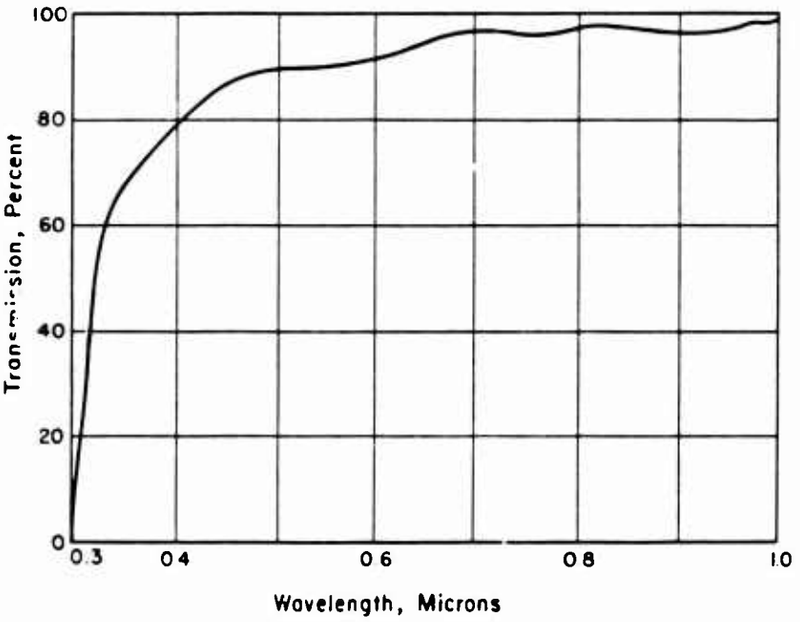

Figure A.7 Atmospheric transmission, Shot Teak.

Appendix B

BLACK BODY RADIATION AT VARIOUS TEMPERATURES

The specific intensity of radiation from an object radiating as a black body at a temperature T is given by Planck's law

$$B_\nu(T) = \frac{2\pi h\nu^3}{c^2} \frac{1}{(e^{h\nu/kT}-1)}$$

Integration of this function over all frequencies yields the Stefan-Boltzmann equation

$$B(T) = \sigma T^4$$

Where: σ has the value 5.6687×10^{-12} watts cm^{-2} $(°K)^{-4}$.

If, for example, the object is a sphere of radius R, then the total power radiated is

$$P = 4\pi R^2 \sigma T^4$$

and the fractional amount radiated in a frequency interval, ν_1 to ν_2 $(\nu_2 > \nu_1)$ is given by

$$f_{1-2} = \left(\frac{15}{\pi^4}\right)\int_{x_1}^{x_2} \frac{x^3\,dx}{(e^x-1)}$$

Where: $x = h\nu/kT$.

By means of the tables in Reference 12, this integral can be determined with a minimum amount of computation.

In this particular case, the long wavelength transmission characteristics of the quartz window that was used in the bolometer required evaluation of this fraction in the regions from 1.0μ to 2.64μ and 2.9μ to 3.6μ. Table B.1 presents the values of xT ($x = h\nu/kT$, $xT = hc/k\lambda$) for wavelengths which pertain to the cutoffs of the dispersion units and the bolometer. For any given temperature the limits on the integral are determined, and hence, the fractional power in this interval.

TABLE B.1 WAVELENGTHS IN MICRONS TRANSFORMED TO xT $(hc/k\lambda)$

$\lambda(\mu)$	xT (°K × 10^4)
0.186	7.735
0.3	4.796
0.4	3.597
0.5	2.878
1.0	1.439
2.64	0.545
2.9	0.496
3.6	0.400

REFERENCES

1. "Handbook of Geophysics"; Revised Edition, 1960; Geophysics Research Directorate, Air Force Research Division, Air Research and Development Command, United States Air Force, L.G. Hanscom Field, Bedford, Massachusetts; The Macmillan Company, New York, New York, and Brett-Macmillan Ltd., Galt, Ontario; Unclassified.

2. F.H. Shelton; "Phenomenology of a High-Altitude Atomic Explosion"; SC-3363 (TR), August 1954; Sandia Corporation, Albuquerque, New Mexico; Secret Restricted Data.

3. H.K. Sen; "A Phenomenological Theory of Scaling of Fireball Minimum Radiant Intensity with Yield and Altitude"; AFCRC-TN-58-[illegible] 1958, Air Force Cambridge Research Center, Bedford, Massachusetts; Secret.

4. H.K. Sen and A.W. Guess; "The Role of Radiation in Shock Propagation with Applications to Altitude and Yield Scaling of Nuclear Fireballs"; AFCRC-TN-59-261, September 1959; Air Force Cambridge Research Center, Bedford, Massachusetts; Secret Restricted Data.

5. M. Annis and J.W. Carpenter; "Estimate of Thermal Pulses from High Altitude Detonations"; ARA-M-6044, April 1958; Allied Research Associates, Inc., Boston, Massachusetts; Secret Restricted Data; Unpublished Private Communication.

6. H.L. Mayer; "Early History of High Altitude Nuclear Explosions"; AFSWC-TR-57-16, May 1957; Air Force Special Weapons Center, Kirtland AFB, New Mexico; Secret Restricted Data.

7. D.E. Buttrey et al.; "Ultrahigh-Altitude Measurement Feasibility Study (Pre-Hardtack Report)"; AFSWC-TN-58-19, August 1958; Air Force Special Weapons Center, Kirtland AFB, New Mexico; Secret Restricted Data.

8. H.L. Brode and F.R. Gilmore; "Estimates of the Thermal Radiation from Nuclear Weapons Burst at High Altitudes"; RM-1938, September 1957; The RAND Corporation, Santa Monica, California; Secret Restricted Data.

9. H.L. Brode; "Theoretical Description of the Early Phases of the Fireball for a Very High Altitude Kiloton Explosion" (U); RM-2247, September 1958; The RAND Corporation, Santa Monica, California; Secret Formerly Restricted Data.

10. H.L. Brode; "Theoretical Description of the Early Phases of the Fireball for a Very High Altitude Megaton Explosion" (U); RM-2249, September 1959; The RAND Corporation, Santa Monica, California; Secret Formerly Restricted Data.

11. F.R. Gilmore; Private Communication 11 July 1958; The RAND Corporation, Santa Monica, California.

12. F.R. Gilmore; "A Table of the Planck Radiation Function and Its Integral" (U); RM-1743, July 1956; The RAND Corporation, Santa Monica, California; Unclassified.

13. P.M. McPherson et al.; "A Photodetecting Instrument with Flat Wavelength Response"; J. Opt. Soc. Am. 51, March 1961; Unclassified.

14. N.J. Kreidl and J.R. Hensler; "Gamma Radiation Insensitive Optical Glass"; J. Opt. Soc. Am. 47, 1957, Page 73; Unclassified.

15. H.E. Stubbs and R.G. Phillips; "High-Speed Bolometer"; Rev. Sci. Instr. 31, 1960, Page 115; Unclassified.

16. R.W. Hillendahl; "Characteristics of Thermal Radiations from Nuclear Weapons"; AFSWP-902, June 1959, Vol I; Armed Forces Special Weapons Project, Washington 25, D.C.; Secret Restricted Data.

17. R.L. Dresser et al.; "Thermal Flux and Albedo Measurements from Aircraft"; Project 5.7, Operation Redwing, WT-1333; Secret Formerly Restricted Data.

18. D.J. Baker and D.E. Thomas; "Nuclear Thermal Pulse Simulator"; Electronics 32, 1959, No. 44, Page 66; Unclassified.

19. E.A. Jones; "Modification of RB-36 Aircraft for Use as Instrument Platforms and Field Measurement of Thermal Energy Resulting from the Detonation of Nuclear and Thermonuclear Devices During Operation Hardtack"; AFCRC-TR-59-298, December 1959; Air Force Cambridge Research Center, Bedford, Massachusetts; Secret Restricted Data.

20. J.W. Reed et al.; "Thermal Radiation from Low-Yield Bursts"; Project 8.8, Operation Hardtack, ITR-1675, January 1959; Air Force Cambridge Research Center, Bedford, Massachusetss; Secret Restricted Data.

21. E.C.Y. Inn et al.; "Early-Time Spectra of Very-High-Altitude Nuclear Detonation" (U); Project 8.4, Operation Hardtack, WT-1650, June 1960; US Naval Radiological Defense Laboratory, San Francisco, California; Secret Restricted Data.

22. "Capabilities of Atomic Weapons" (U); Revised Edition, November 1957, TM-23-200, OPNAV Instruction 03400.1B, AFL 136-1, NAVMC 1104 REV; Armed Forces Special Weapons Project, Washington 25, D.C.; Confidential. (Available through publications channels of Army, Navy, and Air Force.)

23. F.R. Gilmore and A.L. Latter; "Approximate Thermodynamics and Radiation Properties of Air between 2 and 600 Volts" (U); RM-1617, January 1956; The RAND Corporation, Santa Monica, California; ASTIA Document AD-116582; Confidential.

24. F. Fussell and D. Barnes; "Growth of Fireball Radii at Very-High Altitudes" (U); Project 8.3, Operation Hardtack, WT-1649; Edgerton, Germeshausen and Grier, Boston, Massachusetts; Secret Formerly Restricted Data.

25. R. Zirkind; "Narrow-Band Infrared Spectral Irradiance of Very-High Altitude Bursts" (C); Project 8.5, Operation Hardtack, ITR-1651, October 1958; Bureau of Aeronautics, Department of the Navy, Washington, D.C.; Secret Restricted Data.

26. R.C. Jenkins et al.; "Spectral Irradiance History of the Three High Altitude Shots of Operation Hardtack"; AFSWP-1133, USNRDL-TR-333, NS081-001, March 1959; US Naval Radiological Defense Laboratory, San Francisco 24, California; Secret Restricted Data.

27. B. Kivel and K. Bailey; "Tables of Radiation from High Temperature Air"; Research Report 21, December 1957; Avco Research Laboratory, Avco Manufacturing Corporation, Boston, Massachusetts; Unclassified.

28. K. Watanabe; "Ultraviolet Absorption Process in the Upper Atmosphere"; Advances in Geophysics, 1958, H.E. Landberg and J. Van Miegham, Editors; Academic Press, Inc., New York; Unclassified.

29. Friedman, Litchman, and Byram; "Photon Counter Measurements of Solar X-rays and Extreme Ultraviolet Light"; Phys. Rev. 83, 1951, Pages 1025 - 1030; Unclassified.

30. Tousey, Watanabe, and Purcell; "Measurements of Solar Extreme Ultraviolet and X-rays from Rockets by Means of a CA SO_4 : Mn Phosphor"; Phys. Rev. 83, 1951, Pages 792 - 797; Unclassified.

31. J. O. Vann; "An Operational Feasibility Study of an Atomic Weapon Test at or above 100,000 Feet" (U); AFSWC-TR-55-24, December 1955; Air Force Special Weapons Center, Kirtland AFB, New Mexico; Secret.

32. Penndorf, Goldberg, and Lufkin; "Slant Visibility"; Geophysics Research Paper, AFCRC No. 21, 1952; Air Force Cambridge Research Center, Bedford, Massachusetts; Unclassified.

33. Brunt and Kapur; "Quarterly Journal of the Royal Meteorological Society"; 64, 1958, Page 510; Royal Meteorological Society, London; Unclassified.

34. P. F. W. Gotz; "Ozone in the Atmosphere"; Compendium of Meteorology, 1951, Pages 275 - 291, T. F. Malone, Editor; American Meteorological Society, Boston, Massachusetts; Unclassified.

 pages 91 and 92 deleted.